1 **TITLE**

2 The cardiac TRPA1 channel drives calcium-mediated mechano-arrhythmogenesis

3 **AUTHORS**

4 Breanne A. Cameron[1,2]

5 Matthew R. Stoyek[1]

6 Jessi J. Bak[1]

7 Michael S. Connolly[1]

8 Emma A. DeLong[1]

9 Joachim Greiner[2]

10 Rémi Peyronnet[2]

11 Peter Kohl[2,3]

12 *T Alexander Quinn[1,4]

13 **AFFILIATIONS**

14 [1]Department of Physiology and Biophysics, Dalhousie University, Halifax, Canada

15 [2]Institute for Experimental Cardiovascular Medicine, University Heart Center Freiburg · Bad

16 Krozingen and Faculty of Medicine, University of Freiburg, Freiburg, Germany

17 [3]Faculty of Engineering, University of Freiburg, Freiburg, Germany

18 [4]School of Biomedical Engineering, Dalhousie University, Halifax, Canada

19

SUMMARY PARAGRAPH

Maintenance of cardiac function involves a regulatory loop in which electrical excitation causes the heart to contract through excitation-contraction coupling (ECC),[1] and the mechanical state of the heart directly affects its electrical activity through mechano-electric coupling (MEC).[2] However, in pathological states such as acute ischaemia that alter early or late electro-mechanical coordination (*i.e.*, disturbances in ECC or repolarisation-relaxation coupling, RRC), MEC may contribute to the initiation and / or sustenance of arrhythmias (mechano-arrhythmogenesis).[3] The molecular identity of specific factor(s) underlying mechano-arrhythmogenesis in acute ischaemia, however, remain undefined.[4] By rapid stretch of rabbit single left ventricular cardiomyocytes, we show that upon ATP-sensitive potassium channel-induced alterations of RRC, overall vulnerability to mechano-arrhythmogenesis is increased, with mechano-sensitive[5-11] transient receptor potential kinase ankyrin 1 (TRPA1) channels[12] acting as the molecular driver through a Ca^{2+}-mediated mechanism. Specifically, TRPA1 activation drives stretch-induced excitation and creates a substrate for self-sustained arrhythmias, which are maintained by increased cytosolic free Ca^{2+} concentration ($[Ca^{2+}]_i$) and spontaneous $[Ca^{2+}]_i$ oscillations. This TRPA1-dependent mechano-arrhythmogenesis involves microtubules, and can be prevented by block of TRPA1 or buffering of $[Ca^{2+}]_i$. Thus, in cardiac pathologies with disturbed RRC dynamics and / or augmented TRPA1 activity, TRPA1 may represent an anti-arrhythmic target with untapped therapeutic potential.[13-17]

40 **MAIN TEXT**

41 Feedback is an essential element of biological function and fundamental to the adaptation of
42 physiological activity to varying demands. A prime example is found in the heart, an electro-
43 mechanical pump wherein electrical excitation causes mechanical contraction of cardiomyocytes
44 (CM) through a feedforward mechanism involving triggered release of calcium (Ca^{2+}) from
45 intracellular stores, known as excitation-contraction coupling.[1] Feedback in the heart involves
46 effects of the mechanical state of CM on their electrical activity, by a process termed mechano-
47 electric coupling.[2] While this feedback is important for maintaining and fine-tuning normal cardiac
48 function, mechano-electric coupling can also contribute to arrhythmogenesis through
49 mechanically-induced electrophysiological alterations and responses (mechano-
50 arrhythmogenesis).[18]

51 In physiological conditions, the heart is protected from mechano-arrhythmogenesis at all phases
52 of the cardiac cycle, in part through the tight coordination of normal cardiac electro-mechanical
53 activity and transient electrical refractoriness following initiation of the action potential (AP). In
54 disease, disruption of electro-mechanical coordination, haemodynamic overload (either preload or
55 afterload), and / or altered myocardial mechanical properties can elicit arrhythmogenic mechano-
56 electric coupling effects.[3] While the influence of mechano-electric coupling on cardiac
57 electrophysiology in health and disease is well established,[2] the molecular identity of specific
58 driver(s) underlying mechano-arrhythmogenesis is still being explored.[4]

59 Recent results from rabbit isolated heart studies indicate that ventricular mechano-
60 arrhythmogenesis in acute regional ischaemia (as occurs with obstruction of a coronary artery)
61 involves a mechano-sensitive Ca^{2+}-mediated mechanism.[20] The arrhythmogenic role of Ca^{2+} may
62 be facilitated by a pathological disruption of normal electro-mechanical coordination during the

63 late phase of the AP.[20-22] Specifically, ischaemia can induce a dissociation of the otherwise well-
64 synchronised post-excitation recovery of membrane potential and cytosolic free Ca^{2+}
65 concentration ($[Ca^{2+}]_i$). This process, which we henceforth refer to as 'repolarisation-relaxation
66 coupling' (RRC), describes the period in which membrane repolarisation prevents further voltage-
67 mediated trans-sarcolemmal Ca^{2+} influx, and existing cytosolic Ca^{2+} is sequestered into
68 intracellular stores or extruded from the cell, thereby eliciting relaxation. With reduced oxygen
69 availability in ischaemia, activation of ATP-sensitive potassium (K_{ATP}) channels causes rapid
70 cellular repolarisation and an associated shortening of the $[Ca^{2+}]_i$ transient. The resulting decrease
71 in action potential duration (APD) is greater, however, than that in $[Ca^{2+}]_i$ transient duration
72 (CaTD), resulting in a disturbance of normal RRC.[20-22] This may be arrhythmogenic, as it results
73 in the emergence of a potentially vulnerable period (VP_{RRC}) for Ca^{2+}-mediated arrhythmogenesis
74 during late repolarisation, when $[Ca^{2+}]_i$ remains elevated in progressively re-excitable tissue. Such
75 a VP_{RRC} has been shown to occur during beta-adrenergic stimulation in failing human hearts.[23]
76 In the present study, we utilised a cell-level approach that allows for the control of single cell
77 mechanical load with a carbon fibre-based system[19] to investigate the effects of disturbed RRC
78 and the resultant VP_{RRC} on the susceptibility of rabbit left ventricular CM to mechano-
79 arrhythmogenesis. This was combined with fluorescence imaging of trans-membrane voltage and
80 $[Ca^{2+}]_i$, video-based measurement of sarcomere dynamics, and pharmacological interrogation of
81 mechanisms suspected to be involved in triggering and / or sustaining arrhythmic activity upon
82 cell stretch.
83 To mimic ischaemic changes in AP morphology, K_{ATP} channels were activated by application
84 of pinacidil (50 μM, continuous superfusion), a well-established agonist of sulfonylurea receptor
85 (SUR)2A / $K_{ir}6.2$ in cardiac and skeletal muscle.[24] To assess effects of K_{ATP} channel activation on

86 relative post-activation recovery-times of voltage (APD at 50 % repolarisation, APD_{50}) and $[Ca^{2+}]_i$
87 (CaTD at 80 % return to diastolic levels, $CaTD_{80}$), as well as on the duration of the resultant VP_{RRC},
88 we used a single-excitation / dual-emission fluorescence imaging approach.[25] The voltage-
89 sensitive dye di-4-ANBDQPQ and the Ca^{2+}-sensitive dye Fluo-5F, AM (whose high K_d value
90 [~2.3 μM] limits its buffering of near-diastolic $[Ca^{2+}]_i$ and potential artefactual effects on $CaTD_{80}$)
91 were used to simultaneously measure AP and $[Ca^{2+}]_i$ transients in electrically-paced rabbit left
92 ventricular CM under carbon fibre control (Fig. 1a). Upon pinacidil exposure, both APD and CaTD
93 decreased (Fig. 1b, c). The decrease of APD, however, was significantly greater than that of CaTD,
94 resulting in the formation of a cellular VP_{RRC}. This period spans the time during which a CM starts
95 to become re-excitable (repolarisation past APD_{50}) while $[Ca^{2+}]_i$ remains elevated (above $CaTD_{80}$;
96 Fig. 1b, d). This response mimics behaviour previously observed in whole hearts during acute
97 ischaemia,[20,21] as well as with hypoxia alone.[22] After 5 min of pinacidil exposure, there were no
98 further significant alterations in APD, CaTD, or the VP_{RRC} (Fig. 1c, d).

99 Having established a means to reliably evoke a cellular VP_{RRC} by pharmacological K_{ATP}
100 activation, we sought to determine whether normal coordination of electro-mechanical dynamics
101 – as seen in cells exposed to physiological solution (Fig. 1b, c) – protects ventricular CM from
102 mechano-arrhythmogenesis during different phases of the AP (specifically, during late
103 repolarisation and in diastole), and whether disruption of normal RRC increases arrhythmogenic
104 responses to cell stretch. Acute stretch – as occurs in ischaemically weakened myocardium in the
105 whole heart[26] – was applied at three magnitudes with carbon fibres attached to either end of single
106 cells under piezo-electric actuator control (Fig. 2a). Each stretch (average sarcomere stretch levels
107 were 8 ± 1 %, 13 ± 1 %, and 17 ± 1 %) was timed from the electrical pacing stimulus to occur
108 during the VP_{RRC} or in diastole (Fig. 2b, c). Stretch effects were assessed within one and the same

109 cell, exposed to either physiological or pinacidil-containing solutions. Stretch resulted in a variety
110 of changes in cellular mechanical activity (revealed by tracking sarcomere length), including
111 stretch-induced premature contractions (sometimes followed by a second contraction out of sync
112 with the continuing electrical stimulation; Fig. 2d and Supplementary Video 1) and other self-
113 sustained arrhythmic responses. These sustained arrhythmic events included transient
114 refractoriness towards electrical stimulation that resulted in single (Fig. 2e) or multiple (Fig. 2f,
115 Supplementary Video 2) missed beat(s), or sustained activity that either resolved spontaneously
116 (Fig. 2g) or was terminated by application of an additional stretch (Fig. 2h, Supplementary Video
117 3). Arrhythmia incidence was greater in pinacidil-treated cells than in control, both with stretch
118 applied during diastole or the VP_{RRC}. This finding suggests that normal electro-mechanical
119 coordination does indeed protect CM from arrhythmogenesis during late phases of the AP, and
120 that disturbed RRC dynamics increases overall susceptibility to mechano-arrhythmogenesis (Fig.
121 3a).

122 As previous work in the whole heart had shown that the magnitude of tissue deformation is a
123 key determinant of mechano-arrhythmogenesis,[27] we assessed effects of stretch amplitude on
124 arrhythmia incidence. Increasing the piezo-electric actuator displacement amplitude from 20 to
125 40 μm resulted in an increase in the percent sarcomere stretch (along with peak sarcomere length),
126 as well as maximum applied stress (Extended Data Fig. 1). These increases in applied load raised
127 the incidence of stretch-induced arrhythmias in pinacidil-treated cells, while arrhythmia incidence
128 remained low in control cells (Extended Data Fig. 2), indicating that the increase in mechano-
129 arrhythmogenesis that occurs with pinacidil-induced RRC disruption scales with the degree of cell
130 stretch.

131 To assess whether arrhythmias could be the result of stretch-induced cellular damage,
132 contractile function was assessed before and after stretch application of each magnitude. Both in
133 control and in pinacidil-treated cells, diastolic sarcomere length and maximum rate and percent of
134 sarcomere shortening were not significantly different during contractions from resting length,
135 before and after stretch applications of any tested amplitude (Extended Data Fig. 3). These
136 parameters were also not significantly different before and after return to steady state, following
137 periods of self-sustained rhythm disturbances (Extended Data Fig. 4), suggesting that cellular
138 damage may not explain mechano-arrhythmogenesis in our model.

139 We next sought to determine mechanisms underlying the triggering and / or sustenance of
140 cellular mechano-arrhythmogenesis (*i.e.*, stretch-induced single excitations and self-sustained
141 rhythm disturbances) in cells with disturbed RRC. K_{ATP} channels are normally quiescent, but if
142 pre-activated (such as by a reduction in ATP levels during ischaemia or by pinacidil), their open
143 probability is also increased by stretch.[28] As K_{ATP} channels are highly selective for potassium, they
144 have a reversal potential of about -90 mV and conduct an outward current over the entire working
145 range of the ventricular CM membrane potential. As a result, their activation will always contribute
146 to re-/hyperpolarisation. So, K_{ATP} channels may shorten APD, but they cannot account for stretch-
147 induced excitation seen in this and other studies. Interestingly, while pinacidil is generally thought
148 of as a specific activator of K_{ATP} channels, it has been shown to also increase the activity of
149 transient receptor potential kinase ankyrin 1 (TRPA1) channels in HEK293 cells, resulting in a
150 depolarising trans-membrane current and Ca^{2+} influx.[29] Importantly in the context of mechano-
151 arrhythmogenesis, TRPA1 channels: (i) are inherently mechano-sensitive[5] and contribute to
152 mechanically-evoked electrical responses (measured as trans-membrane currents and deduced
153 from AP initiation) in sensory neurons,[6-8] astrocytes,[9] and vertebrate hair cells;[10] (ii) have been

154 found to be functionally expressed in murine ventricular CM[30] (although not all studies have found
155 this)[31] and to drive changes in *Drosophila* heart rhythm in response to mechanical stimulation;[11]
156 and (iii) are important for cardiovascular function and disease progression.[13] We hypothesised that,
157 if TRPA1 channels are functionally expressed in rabbit left ventricular CM, then they could
158 contribute to the increase in mechano-arrhythmogenesis seen with pinacidil treatment.

159 To assess the presence and function of TRPA1 channels in the rabbit left ventricle, we first
160 measured TRPA1 protein expression in tissue from the left ventricular free wall by Western
161 blotting, which revealed robust expression (Extended Data Fig. 5a). Next, functional expression
162 of TRPA1 channels in left ventricular CM was evaluated by measuring ion channel activity in cell-
163 attached patches during application of the TRPA1 channel-specific agonist, allyl isothiocyanate
164 (AITC; 50 μM).[32] AITC exposure caused an increase in total inward current, while there was no
165 significant change in time-matched control cells (Extended Data Fig. 5b, c).

166 Having shown that TRPA1 channels are functionally expressed in rabbit ventricular CM, we
167 explored their possible involvement in the mechano-arrhythmogenesis observed in our model. This
168 was done by applying either a non-specific blocker of cation non-selective mechano-sensitive ion
169 channels (streptomycin;[33] 50 μM), or a specific TRPA1 channel blocker (HC-030031;[34] 10 μM,
170 which has been shown to inhibit TRPA1 current and mechanically-induced excitation in sensory
171 neurons[6-8]) to pinacidil-treated cells. Streptomycin and HC-030031 reduced the incidence of
172 cellular arrhythmias with pinacidil treatment, both with stretch during diastole and in the VP_{RRC}
173 (Fig. 3a; arrhythmia incidence remained low in control cells, Extended Data Fig. 6). This finding
174 suggests that mechano-sensitive channels are involved in mechano-arrhythmogenesis across
175 phases of the AP when there is disruption of normal electro-mechanical coordination. More
176 specifically, with disruption of RRC, mechano-sensitive channels appear to contribute to the

177 increase in both single triggers and self-sustained rhythm disturbances, as their block (compared
178 in pooled data from diastolic and VP_{RRC} stretches in cells exposed to streptomycin- or HC-030031)
179 in pinacidil-treated cells was able to prevent the increase of both classifications of arrhythmias
180 (Fig. 3a, inset; incidence remained low in control cells, Extended Data Fig. 6). Importantly,
181 streptomycin and HC-030031 appeared to have no other functional effects, as there was no
182 significant change in diastolic sarcomere length or contractile function with their application to
183 control cells (Extended Data Fig. 7).

184 Next, as activation of TRPA1 channels is known to increase Ca^{2+} influx,[12,35] we assessed
185 whether cytosolic Ca^{2+} contributes to the mechano-arrhythmogenesis seen in our study. This was
186 achieved by buffering cytosolic Ca^{2+} with BAPTA-AM (1 μM, $K_d \approx 0.5$ μM), which has
187 previously been shown in ventricular CM to prevent stretch-induced changes in cardiac
188 electrophysiology driven by changes in $[Ca^{2+}]_i$.[36] In pinacidil treated cells, BAPTA-AM reduced
189 arrhythmia incidence with stretch both during diastole and in the VP_{RRC}. As stretch is also known
190 to increase sarcoplasmic reticulum Ca^{2+} leak through ryanodine receptors[37] (an effect that is
191 enhanced in ischaemia[38]), we investigated its possible contribution to the dependence of mechano-
192 arrhythmogenesis on cytosolic Ca^{2+} by stabilising ryanodine receptors in their closed state with
193 dantrolene (1 μM, which has been shown to not affect Ca^{2+}-induced Ca^{2+} release or contraction[39]).
194 However, dantrolene had no significant effect on the incidence of stretch-induced arrhythmias,
195 suggesting that Ca^{2+} influx *via* TRPA1, but not mechano-sensitive Ca^{2+} release from the
196 sarcoplasmic reticulum, is involved in mechano-arrhythmogenesis (Fig. 3a). Yet, in contrast to
197 mechano-sensitive channels, which contribute to both single triggers and self-sustained rhythm
198 disturbances in pinacidil-treated cells, cytosolic Ca^{2+} appears to be involved only in the observed
199 increase in self-sustained rhythm disturbances, as BAPTA-AM did not decrease the incidence of

200 single excitations (compared in pooled data from diastolic and VP_{RRC} stretches in BAPTA-AM-
201 treated cells; Fig. 3a, inset). In control cells treated with either BAPTA-AM or dantrolene, the
202 incidence of stretch-induced arrhythmias remained low (Extended Data Fig. 6) and there was no
203 significant change in diastolic sarcomere length or maximum rate of systolic sarcomere shortening.
204 There was, however, a significant decrease in the percent systolic sarcomere shortening with both
205 interventions, presumably due to a reduction in peak systolic $[Ca^{2+}]_i$ (by buffering with BAPTA-
206 AM or reduced sarcoplasmic reticulum Ca^{2+} release with dantrolene; Extended Data Fig. 7).

207 We then sought to more specifically explore whether TRPA1 channels are indeed a source of
208 mechano-arrhythmogenesis. Control cells were exposed to AITC (10 μM), which enhances the
209 response of TRPA1 channels to mechanical stimulation,[8] and then subjected to diastolic stretch (as
210 there was no K_{ATP}-induced disturbance of RRC in these cells, no VP_{RRC} stretch was applied). AITC
211 caused an increase in both stretch-induced single excitations and self-sustained events compared
212 to control cells (Fig. 3b). As with pinacidil exposure, application of HC-030031 to AITC-treated
213 cells prevented this increase in mechano-arrhythmogenesis. However, unlike in pinacidil-treated
214 cells, BAPTA-AM also prevented the increase in both types of rhythm disturbances during AITC
215 exposure (Fig. 3b, inset).

216 While the above findings strongly suggest a role of TRPA1 channels in mechano-
217 arrhythmogenesis, we did not find an increase in TRPA1 current in our patch-clamp experiments
218 when the cell membrane within the pipette was stretched by negative pressure application. As there
219 is a large body of evidence demonstrating that interactions between TRP channels and
220 microtubules are important for TRP channel function,[40] we hypothesised that microtubule-
221 mediated mechano-transduction during axial cell stretch may be necessary for a mechanically-
222 induced response, which would not have been engaged during local membrane stretch *via* the patch

223 pipette. To test for the importance of microtubules in TRPA1-dependent mechano-
224 arrhythmogenesis, cells were exposed to paclitaxel (10 μM) to increase polymerisation and
225 stabilisation of microtubules,[41] which has been shown to increase the probability of stretch-induced
226 arrhythmias in isolated rabbit hearts.[42] Immunofluorescence imaging revealed that paclitaxel
227 increased the density of the microtubule network (Extended Data Fig. 8a-c), which was associated
228 with an increased incidence of single excitations upon stretch in diastole (Extended Data Fig. 8d).
229 That this increase in mechano-arrhythmogenesis involves interactions with TRPA1 channels was
230 supported by a reduction in the incidence of stretch-induced arrhythmias in paclitaxel -treated cells
231 during block of TRPA1 with HC-030031 (Extended Data Fig. 8d).

232 Our results up to this point suggest that an inward current, passing (at least in part) through
233 mechano-sensitive TRPA1 channels, acts as a trigger for stretch-induced excitations and
234 contributes to a substrate for self-sustained rhythm disturbances. While a transient inward
235 depolarising current with stretch may explain the role of TRPA1 in single excitations, its
236 contribution to the formation of an arrhythmogenic substrate for self-sustained rhythm
237 disturbances warranted further investigation. TRPA1 channel activity has been shown to cause an
238 increase in diastolic $[Ca^{2+}]_i$ in ventricular CM.[43] This increase in diastolic $[Ca^{2+}]_i$ can contribute to
239 sarcoplasmic reticulum Ca^{2+} release, creating an arrhythmogenic substrate,[44] and can further
240 activate TRPA1 channels.[45] We therefore hypothesised that TRPA1-mediated effects on $[Ca^{2+}]_i$
241 may account for the observed increase in stretch-induced self-sustained rhythm disturbances. We
242 measured $[Ca^{2+}]_i$ with a ratiometric fluorescence imaging technique (using the Ca^{2+}-sensitive dye
243 Fura Red, AM; $K_d \approx 400$ nM), which showed that both pinacidil and AITC application increase
244 $[Ca^{2+}]_i$ in diastole (Extended Data Fig. 9). However, despite the anti-arrhythmic effect of blocking
245 TRPA1 channels both in AITC and in pinacidil-treated cells, HC-030031 reduced the increase in

246 diastolic $[Ca^{2+}]_i$ only during AITC treatment (Extended Data Fig. 9). This finding suggests that the
247 increase in diastolic $[Ca^{2+}]_i$ with AITC and pinacidil may be occurring through different
248 mechanisms. As chelating cytosolic Ca^{2+} with BAPTA-AM was also anti-arrhythmic in both
249 pinacidil- and AITC-treated cells (Fig. 3a, b), this suggests that increased $[Ca^{2+}]_i$ may be necessary
250 for sustenance, but not sufficient for induction of mechano-arrhythmogenesis. Unfortunately, we
251 could not measure the effects of BAPTA-AM on $[Ca^{2+}]_i$, as the combined buffering of Ca^{2+} by
252 BAPTA-AM and the Ca^{2+}-sensitive dye Fura Red greatly diminished cell contraction.

253 Explicit evidence for a direct role of Ca^{2+} in the self-sustained rhythm disturbances came from
254 dual voltage-Ca^{2+} fluorescence imaging, which revealed an increase in $[Ca^{2+}]_i$, along with Ca^{2+}
255 oscillations that precede changes in voltage, indicating that oscillations in $[Ca^{2+}]_i$ can drive
256 sustained aberrant electrical behaviour (Fig. 4a, Supplementary Video 4). It is worth noting here
257 that changes in repolarisation can also destabilise the electrical activity of ventricular CM. Thus,
258 in pinacidil-treated cells, a stretch-induced increase in K_{ATP} channel current may have directly
259 contributed to the ability to sustain arrhythmic activity by shortening APD, thereby increasing the
260 diastolic interval and the duration of the excitable period between paced beats.[28]

261 Finally, with an increase in $[Ca^{2+}]_i$, there is the possibility that a change in cellular mechanics
262 may also contribute to mechano-arrhythmogenesis by enhancing mechano-transduction or altering
263 the characteristics of stretch. However, we observed no significant effect of pinacidil on diastolic
264 or systolic cell stiffness, measured (respectively) as the slopes of end-diastolic and end-systolic
265 stress-sarcomere length relationship in mechanically loaded (*via* carbon fibres) contracting cells
266 (Extended Data Fig. 10). Furthermore, we found no significant effect of pinacidil on percent
267 sarcomere stretch, stretched sarcomere length, or maximum applied stress during stretch (Extended
268 Data Fig. 1). This suggests that changes in cellular mechanics may not be a major contributor to

269 observed effects (note: there was a significant shift in the stiffness curves to the right in pinacidil-
270 treated cells, which may relate to reduced affinity of myofilaments for Ca^{2+} through TRPA1-
271 induced phosphorylation of troponin I;[43] Extended Data Fig. 10). In a subset of pinacidil-treated
272 cells for which two consecutive stretches of the same magnitude (occurring either during diastole
273 or the VP_{RRC}) first did, and then did not, result in an arrhythmia, the characteristic effects of each
274 stretch were not significantly different (Extended Data Fig. 11), suggesting that passive cell
275 mechanical properties were not affected by acute stretch application.

276 Taken together, our results suggest that TRPA1 channels contribute both to acute triggering and
277 to Ca^{2+}-mediated sustenance of ventricular mechano-arrhythmogenesis. Figure 4b summarises our
278 findings and presents a working model of TRPA1's role in triggering stretch-induced excitation
279 (through a depolarising trans-sarcolemmal current) and in creating a substrate for sustained
280 arrhythmic activity (through increased diastolic $[Ca^{2+}]_i$).

281 TRPA1 channels are mechano-sensitive and thus allow for a trans-sarcolemmal influx of
282 cations upon stretch (specifically Ca^{2+} when TRPA1 channels are pre-activated),[12,35] which
283 depolarises membrane potential. An increase in $[Ca^{2+}]_i$ may result in further membrane
284 depolarisation *via* electrogenic forward-mode sodium-Ca^{2+} exchanger activity.[44] If the
285 depolarisation is sufficiently large, it will cause excitation and premature contraction of the cell,
286 with arrhythmic activity sustained if $[Ca^{2+}]_i$ remains sufficiently elevated for a period of time.
287 Importantly, TRPA1 channel activity is directly modulated by $[Ca^{2+}]_i$. Specifically, an increase in
288 $[Ca^{2+}]_i$ potentiates TRPA1 channel activity, but at a certain level of $[Ca^{2+}]_i$ TRPA1 channels are
289 progressively inactivated, thus limiting the degree of Ca^{2+} overload and, perhaps, preventing lethal
290 cell damage.[46] In our experiments, exposure to AITC caused direct activation of TRPA1 channels

291 and subsequent diastolic $[Ca^{2+}]_i$ loading, while pinacidil either directly activated TRPA1 channels,
292 or did so indirectly *via* an increase in $[Ca^{2+}]_i$.

293 In conclusion, our results suggest that TRPA1 activation leads to enhanced microtubule-
294 dependent, stretch-induced depolarising currents and increased $[Ca^{2+}]_i$. As such, block of TRPA1
295 channels reduces both the triggering and self-sustenance of mechano-arrhythmogenesis, while
296 buffering diastolic $[Ca^{2+}]_i$ only reduces arrhythmia sustenance. These findings have potentially
297 important implications for anti-arrhythmic strategies in cardiac pathologies associated with
298 augmented TRPA1 channel expression or activity.[13] This is especially true for cases in which
299 additional factors activate TRPA1 channels (*e.g.*, oxidative stress),[47] as the response of TRPA1 to
300 mechanical stimulation is enhanced by an increase in their baseline activity.[8] For instance, acute
301 myocardial ischaemia is associated with TRPA1-mediated myocardial damage[14] (which can be
302 reduced by TRPA1 inhibition[15]), along with lethal ventricular arrhythmias that are thought to
303 involve contributions of altered tissue mechanics, intracellular Ca^{2+} handling, and oxidative
304 stress.[26] Thus, targeting TRPA1 channels in that setting may help in preventing multiple
305 detrimental outcomes. This could also be true in chronic pathologies in which lethal arrhythmias
306 occur, and which are associated with changes in cardiac mechanics, intracellular Ca^{2+} dynamics,
307 oxidative stress, and other TRPA1 modulating factors,[12] such as ventricular pressure overload. In
308 keeping with this suggestion, TRPA1 inhibition in chronic hypertension has been shown to reduce
309 hypertrophy and fibrosis.[16] Overall, these observations, combined with our current findings,
310 suggest TRPA1 channels may represent a novel, underappreciated anti-arrhythmic target with
311 exciting therapeutic potential.[17]

312

313 **MAIN REFERENCES**

314 1. Bers, D. M. Cardiac excitation-contraction coupling. *Nature*. **415**, 198-205 (2002).

315 2. Quinn, T. A. & Kohl, P. Cardiac mechano-electric coupling: acute effects of mechanical
316 stimulation on heart rate and rhythm. *Physiol. Rev.* **101**, 37-92 (2021).

317 3. Quinn, T. A. The importance of non-uniformities in mechano-electric coupling for ventricular
318 arrhythmias. *J. Interv. Card. Electrophysiol.* **39**, 25-35 (2014).

319 4. Peyronnet, R., Nerbonne, J. M. & Kohl, P. Cardiac mechano-gated ion channels and
320 arrhythmias. *Circ. Res*. **118**, 311-29 (2016).

321 5. Moparthi, L. & Zygmunt P. M. Human TRPA1 is an inherently mechanosensitive bilayer-
322 gated ion channel. *Cell Calcium* **91**, 102255 (2020).

323 6. Kerstein, P.C., del Camino, D., Moran, M. M. & Stucky, C. L. Pharmacological blockade of
324 TRPA1 inhibits mechanical firing in nociceptors. *Mol. Pain* **5**, 19 (2009).

325 7. Vilceanu, D. & Stukcy, C. L. TRPA1 mediates mechanical currents in the plasma membrane
326 of mouse sensory neurons. *PLoS One* **5**, e12177 (2010).

327 8. Brierly S. M., *et al*. TRPA1 contributes to specific mechanically activated currents and
328 sensory neuron mechanical hypersensitivity. *J. Physiol*. **589**, 3575-93 (2011).

329 9. Oh, S-J. *et al*. Ultrasonic neuromodulation via astrocytic TRPA1. *Curr. Biol*. **29**, 3386-401
330 (2019).

331 10. Corey, D. P., *et al*. TRPA1 is a candidate for the mechanosensitive transduction channel of
332 vertebrate hair cells. *Nature* **432**, 723-30 (2004).

333 11. Sénatore S., Reddy, V. R., Sémériva, M., Perrin, L. & Lalevée, N. Response to mechanical
334 stress is mediated by the TRPA channel painless in the *Drosophila* heart. *PLoS Genet.* **6**,
335 e1001088 (2010).

336 12. Meents, J. E., Ciotu, C. I. & Fischer, M. J. M. TRPA1: a molecular view. *J. Neurophysiol.*
337 **121**, 427-443 (2019).
338 13. Wang, Z. *et al*. The TRPA1 channel in the cardiovascular system: promising features and
339 challenges. *Front*. *Pharmacol.* **10**, 1253 (2019).
340 14. Conklin, D. J., *et al*. TRPA1 channel contributes to myocardial ischemia-reperfusion injury.
341 *Am. J. Physiol. Heart. Circ. Physiol.* **316**, H889-99 (2019).
342 15. Li, R., Liu, R., Yan, F., Zhuang, X., Shi, H. & Gao, X. Inhibition of TRPA1 promotes cardiac
343 repair in mice after myocardial infarction. *J. Cardiovasc. Pharmacol.* **75**, 240-9 (2020).
344 16. Wang, Z. *et al*. TRPA1 inhibition ameliorates pressure overload-induced cardiac hypertrophy
345 and fibrosis in mice. *E. Bio. Medicine* **36**, 54-62 (2018).
346 17. Moran, M. M. TRP channels as potential drug targets. *Annu. Rev. Pharmacol. Toxicol.* **58**,
347 309-30 (2018).
348 18. Quinn, T. A. Cardiac mechano-electric coupling: a role in regulating normal function of the
349 heart? *Cardiovasc. Res*. **108**, 1-3 (2015).
350 19. Iribe, G., Helmes, M. & Kohl, P. Force-length relations in isolated intact cardiomyocytes
351 subjected to dynamic changes in mechanical load. *Am. J. Physiol. Circ. Physiol.* **292**, H1487-
352 97 (2007).
353 20. Baumeister, P., *et al.* Mechanically-induced ventricular arrhythmias during acute regional
354 ischemia. *J. Mol. Cell. Cardiol*. **124,** 87-8 (2018).
355 21. Tang, L., Joung, B., Ogawa, M., Chen, P. S. & Lin S. F. Intracellular calcium dynamics,
356 shortened action potential duration, and late-phase 3 early afterdepolarization in Langendorff-
357 perfused rabbit ventricles. *J. Cardiovasc. Electrophysiol.* **12**, 1364-71 (2012).

358 22. Takahashi, M., Yokoshiki, H., Mitsuyama, H., Watanabe, M., Temma, T., Kamada, R.,
359 Hagiwara, H., Takahashi, Y., Anzai, T. SK channel blockade prevents hypoxia-induced
360 ventricular arrhythmias through inhibition of Ca^{2+}/voltage uncoupling in hypertrophied hearts.
361 *Am. J. Physiol. Heart. Circ. Physiol*. **320**, H1456-69 (2021).
362 23. Lang, D., *et al*. Arrhythmogenic remodeling of β_2 versus β_1 adrenergic signaling in the human
363 failing heart. *Circ. Arrhythm. Electrophysiol.* **8**, 409-19 (2015).
364 24. Fujita, A. & Kurachi, Y. Molecular aspects of ATP-sensitive K^+ channels in the cardiovascular
365 system and K^+ channel openers. *Pharmacol. Ther.* **85**, 39-53 (2000).
366 25. Quinn, T. A., *et al*. Electrotonic coupling of excitable and nonexcitable cells in the heart
367 revealed by optogenetics. *Proc. Natl. Acad. Sci. U S A.* **113**:14852-7 (2016).
368 26. Carmeliet, E. Cardiac ionic currents and acute ischemia: from channels to arrhythmias.
369 *Physiol. Rev.* **79**, 917-87 (1999).
370 27. Quinn, T. A., Jin, H., Lee, P. & Kohl, P. Mechanically induced ectopy via stretch-activated
371 cation-nonselective channels is caused by local tissue deformation and results in ventricular
372 fibrillation if triggered on the repolarization wave edge (*Commotio cordis*). *Circ. Arrhythm.*
373 *Electrophysiol*. **10**, e004777 (2017).
374 28. Van Wagoner, D. R. Mechanosensitive gating of atrial ATP-sensitive potassium channels.
375 *Circ. Res.* **72**: 973–83 (1993).
376 29. Ma, L. H., *et al*. Pinacidil, a K_{ATP} channel opener, identified as a novel agonist for TRPA1.
377 *Chinese Sci. Bull.* **57**, 1810-7 (2012).
378 30. Andrei, S. R., Sinharoy, P., Bratz, I. N. & Damron, D. S. TRPA1 is functionally co-expressed
379 with TRPV1 in cardiac muscle: co-localization at z-discs, costameres and intercalated discs.
380 *Channels* **10**, 395-409 (2016).

381 31. Hoebart, C., Rojas-Galvan, N. S., Ciotu, C. I., Aykac, I., Reissig, L. F., Weninger, W. J., Kiss,
382 A., Podesser, B. K., Fischer, M. J. M., Heber, S. No functional TRPA1 in cardiomyocytes.
383 *Acta. Physiol. (Oxf.)* **5**, e13659 (2021).
384 32. Jordt, S-E., *et al*. Mustard oils and cannabinoids excite sensory nerve fibres through the TRP
385 channel ANKTM1. *Nature*. **427**, 260-5 (2004).
386 33. White, E. Mechanosensitive channels: therapeutic targets in the myocardium? *Curr Pharm*
387 *Des*. **12**, 3645-63 (2006).
388 34. McNamara, C. R. *et al*. TRPA1 mediates formalin-induced pain. *Proc. Natl. Acad. Sci. U S*
389 *A.* **104**,13525-30 (2007).
390 35. Nilius, B., Appendino, G., & Owsianik, G. Bobkov, Y. V., Corey, E. A, & Ache, B. W. The
391 transient receptor potential channel TRPA1: from gene to pathophysiology. *Pflugers Arch.*
392 **464**, 425-58 (2012).
393 36. Calaghan, S. C., Belus, A., White, E. Do stretch-induced changes in intracellular calcium
394 modify the electrical activity of cardiac muscle? *Prog. Biophys. Mol. Biol.* **82**, 81-95 (2003).
395 37. Iribe, G. *et al.* Axial stretch of rat single ventricular cardiomyocytes causes an acute and
396 transient increase in Ca^{2+} spark rate. *Circ Res* **104**, 787–795 (2009).
397 38. Cameron, B. A., Kai, H., Kaihara, K., Iribe, G. & Quinn, T. A. Ischemia enhances the acute
398 stretch-induced increase in calcium spark rate in ventricular myocytes. *Front Physiol* **11**, 289
399 (2020).
400 39. Hartmann, N., *et al*. Antiarrhythmic effects of dantrolene in human diseased cardiomyocytes.
401 *Heart Rhythm* **14**, 412-9 (2017).

402 40. Smani, T., Dionisio, N., López, J. J., Berna-Erro, A., Rosado, J. A. Cytoskeletal and
403 scaffolding proteins as structural and functional determinants of TRP channels. *Biochim.*
404 *Biophys. Acta.* **1838**, 658-64 (2014).
405 41. Schiff, P. B., Fant, J., Horwitz, S. B. Promotion of microtubule assembly in vitro by taxol.
406 *Nature* **277**, 665-7 (1979).
407 42. Parker, K. K., Taylor, L. K., Atkinson, J. B., Hansen, D. E., Wikswo, J. P. The effects of
408 tubulin-binding agents on stretch-induced ventricular arrhythmias. *Eur. J. Pharmacol*. **417**,
409 131-40 (2001).
410 43. Andrei, S. R. *et al*. TRPA1 ion channel stimulation enhances cardiomyocyte contractile
411 function via a CaMKII-dependent pathway. *Channels* **11**, 587-603 (2017).
412 44. Landstrom, A. P., Dobrev D. & Wehrens, X. H. T. Calcium signaling and cardiac arrhythmias.
413 *Circ. Res.* **120**, 1969-93 (2017).
414 45. Zurborg, S., Yurgionas, B., Jira, J. A., Caspani, O. & Heppenstall, P. A. Direct activation of
415 the ion channel TRPA1 by Ca^{2+}. *Nat. Neurosci.* **10**, 277-9 (2007).
416 46. Wang, Y. Y., Chang R. B., Waters, H. N., McKemy, D. D. & Liman, E. R. The nociceptor ion
417 channel TRPA1 is potentiated and inactivated by permeating calcium ions. *J. Biol. Chem.* **21**,
418 32691-32703 (2008).
419 47. Andersson, D. A., Gentry, C., Moss, S. & Bevan, S. Transient receptor potential A1 is a
420 sensory receptor for multiple products of oxidative stress. *J. Neurosci.* **28**, 2485-94 (2008).
421

FIGURES

Figure 1 | Disruption of repolarisation-relaxation coupling (RRC) in rabbit isolated left ventricular cardiomyocytes by activation of ATP-sensitive potassium channels with pinacidil. a, Schematic of the single-excitation/dual-emission fluorescence imaging approach, utilising a single camera-image splitter system. **b,** Representative traces of action potentials (AP, blue) and calcium transients (CaT, red), simultaneously recorded by fluorescence imaging in a single ventricular cardiomyocyte before (left) and after (right) 5 min of pinacidil exposure (50 µM, to activate ATP-sensitive potassium channels), showing RRC disruption. The associated vulnerable period (VP_{RRC}; highlighted in green) is the interval during which cardiomyocytes start to become re-excitable, while cytosolic calcium concentration ($[Ca^{2+}]_i$) remains elevated (calculated as the difference between the time of recovery of cytosolic Ca^{2+} to 80 % [$CaTD_{80}$, red dashed line] and membrane potential to 50 % [APD_{50}, blue dashed line] of diastolic levels), plus the excitation contraction coupling time (ECC). **c,** APD_{50} (blue), $CaTD_{80}$ (red), and **d**, VP_{RRC} duration (green) during 10 min of Tyrode (NT, solid) or pinacidil (PIN, dashed) superfusion. Differences assessed by one-way ANOVA with Tukey *post-hoc* tests. *$p < 0.05$ for NT compared to PIN; †$p < 0.05$ for the change within either NT or PIN over time; #$p < 0.05$ for the change over time of APD_{50} compared to $CaTD_{80}$. Error bars represent standard error of the mean. N = rabbits / group, n = cells / group.

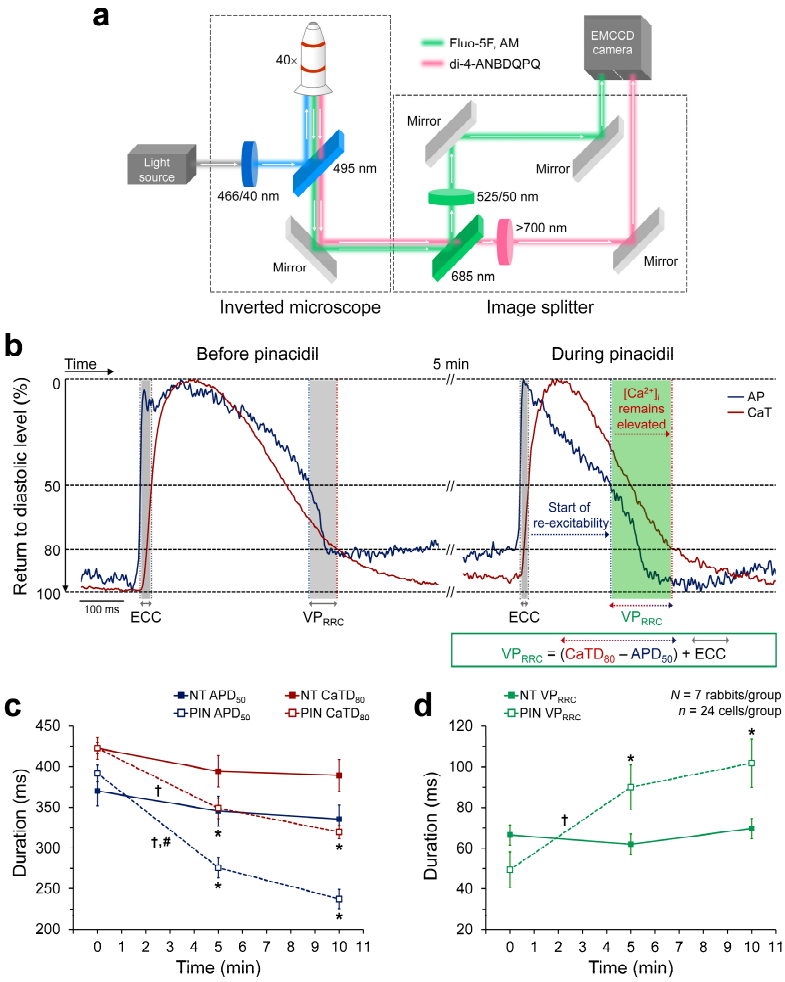

Figure 2 | Arrhythmias elicited by acute stretch of rabbit single left ventricular cardiomyocytes. a, Representative brightfield image of a ventricular cardiomyocyte before (left) and during (right) axial stretch, applied using a carbon fibre-based system. Scale bar: 10 µm. **b**, Schematic of the stretch protocol. **c**, Representative measurement of sarcomere length in a cell exposed to pinacidil (50 µM, to activate ATP-sensitive potassium channels) during 1 Hz pacing (orange dots) and stretched (green segments of trace) in diastole (stretches 1 and 3) or during the vulnerable period (VP_{RRC}, stretches 2 and 4), which did not result in an arrhythmia (normal paced rhythm, NPR, was maintained). **d,** Premature contraction (blue segment) upon VP_{RRC}-timed stretch. **e,** Refractoriness after a diastolic stretch. **f** premature contraction after a diastolic stretch, followed by refractoriness and multiple missed beats (red segment). **g,** Self-sustained arrhythmic activity (red segment) after a VP_{RRC}-timed stretch that spontaneously resolved. **h,** Self-sustained arrhythmic activity (red segment) after a diastolic stretch that was terminated by an additional stretch (second green bar).

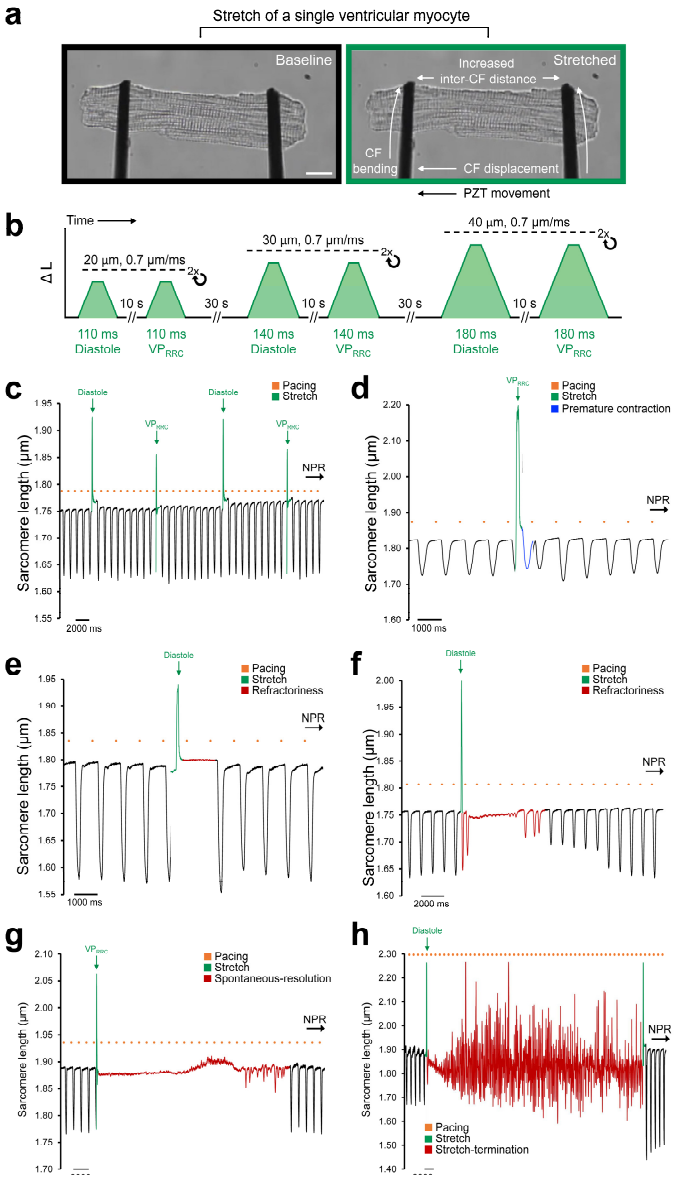

Figure 3 | Effects of pharmacological interventions on mechano-arrhythmogenesis. a, Incidence of arrhythmias (purple) in rabbit isolated left ventricular cardiomyocytes with acute stretch applied during diastole or the vulnerable period (VP_{RRC}) in cells exposed to one of the following treatments: Tyrode (NT); pinacidil (PIN, 50 μM, to activate ATP-sensitive potassium channels); PIN + streptomycin (STP, 50 μM, to additionally non-specifically block mechano-sensitive channels, MSC); PIN + HC-030031 (10 μM, to additionally block TRPA1 channels); PIN + BAPTA (1 μM, to additionally buffer cytosolic Ca^{2+}, $[Ca^{2+}]_i$) or PIN + dantrolene (DNT, 1 μM, to additionally stabilise ryanodine receptors). **Inset:** of the total arrhythmia incidence (measured as the sum of diastolic and VP_{RRC} incidence), the proportion of arrhythmias that were premature contractions (blue, left) or self-sustained arrhythmic events (shades of red, right), and the effect of blocking either MSC (measured as the pooled data from stretches in the PIN + STP and PIN + HC-030031 interventions) or chelating $[Ca^{2+}]_i$ (measured as the pooled data from stretches in the PIN + BAPTA intervention) on their incidence in cells with activated ATP-sensitive potassium channels. Differences assessed using chi-square contingency tables and Fisher's exact test. $*p < 0.05$, $**p < 0.01$, $***p < 0.001$ for diastole; $\#p < 0.05$, $\#\#p < 0.01$, $\#\#\#p < 0.001$ for VP_{RRC}. **b**, Incidence of arrhythmias with stretch during diastole in cells exposed to one of the following treatments: NT; allyl isothiocyanate (AITC, 10 μM, to activate TRPA1 channels); AITC + HC-030031; or AITC + BAPTA. **Inset:** of the total diastolic arrhythmia incidence, the proportion of those that were premature contractions (blue, left) or self-sustained arrhythmic events (shades of red, right), and the effect of blocking MSC (measured as the AITC + HC-030031 intervention) or chelating $[Ca^{2+}]_i$ (measured as the AITC + BAPTA intervention) on their incidence in cells with activated TRPA1 channels. Differences assessed using chi-square contingency tables and Fisher's exact test. $*p < 0.05$, $**p < 0.01$, $***p < 0.001$. N = rabbits / group, n = cells / group, m = stretch stimuli applied.

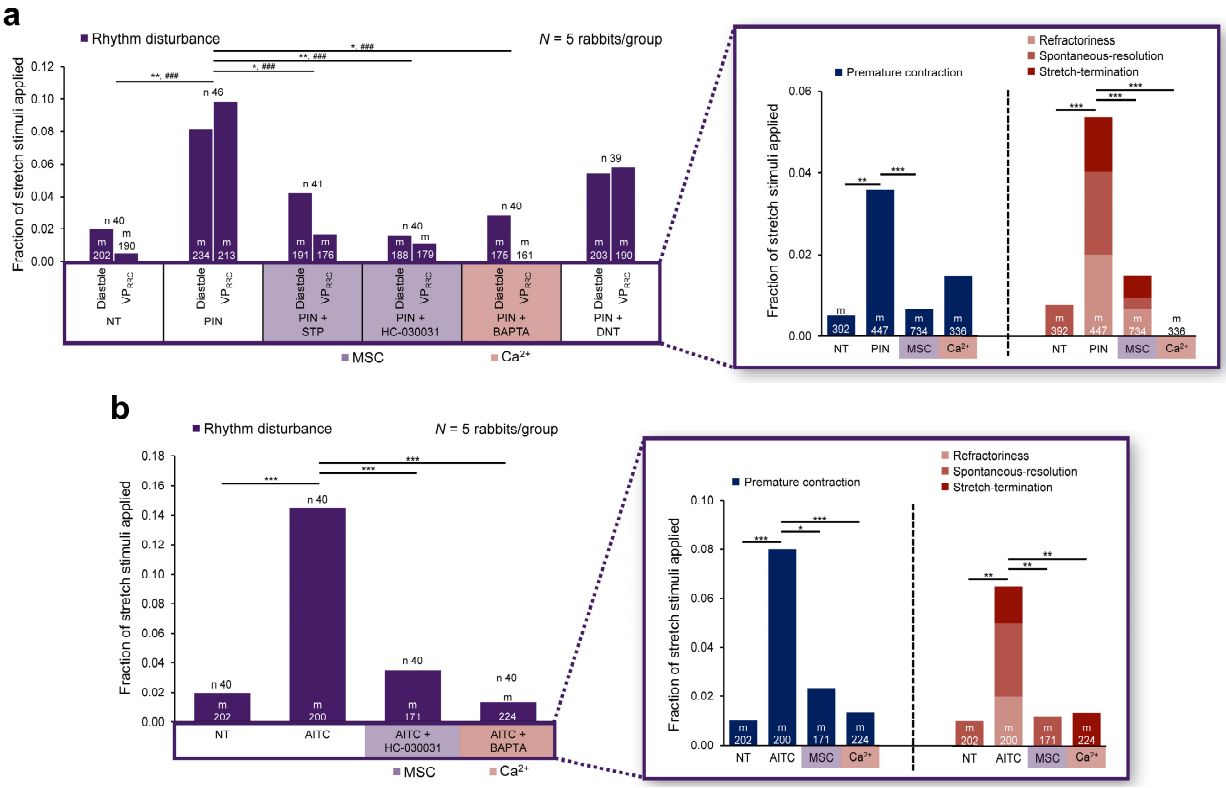

Figure 4 | Role of TRPA1 channels and cytosolic calcium ($[Ca^{2+}]_i$) in ventricular mechano-arrhythmogenesis. a, Example trace of voltage (blue) and $[Ca^{2+}]_i$ (red), simultaneously recorded by fluorescence imaging in a rabbit isolated left ventricular cardiomyocyte exposed to pinacidil (PIN, 50 µM, to activate K_{ATP} channels). Rapid stretch in the vulnerable period (VP_{RRC}, green) resulted in sustained arrhythmic activity, initiated by sustained depolarisation and an associated increase in $[Ca^{2+}]_i$ above normal systolic levels, prompting spontaneous oscillations in $[Ca^{2+}]_i$ (which subsequently resolved, followed by normal paced beats; not shown). **Blue inset**: Scaled voltage and Ca^{2+} fluorescence curves (top) and phase plot of the first beat (bottom) showing that, prior to stretch, changes in voltage preceded Ca^{2+}. **Red inset**: Scaled voltage and Ca^{2+} fluorescence curves (top) and phase plot of the first beat (bottom) showing $[Ca^{2+}]_i$ oscillations preceding changes in voltage during sustained arrhythmia after stretch, suggesting aberrant Ca^{2+} handling as a driving mechanism. **b,** Schematic representation of mechanisms underlying TRPA1 channel driven mechano-arrhythmogenesis. Effects of stretch (black) on cell electrophysiology (blue), Ca^{2+} (red), or a combination of stretch and Ca^{2+} (purple). TRPA1 agonists (green) and targets of pharmacological antagonists (orange) are indicated. AITC, Allyl isothiocyanate; NCX, Na^+-Ca^{2+} exchanger; PIN, pinacidil; STP, streptomycin; TAX, paclitaxel.

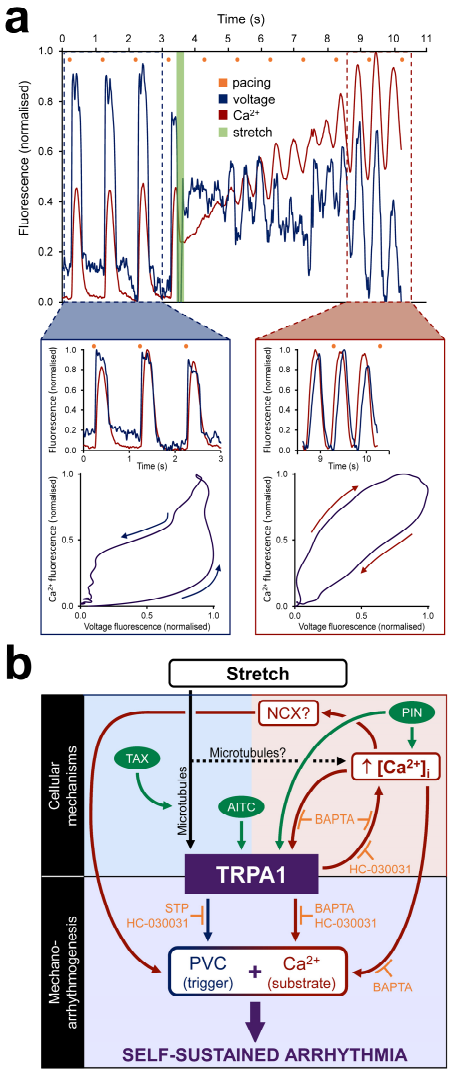

504 **METHODS**

505 **Animal model.** Experiments involved the use of female New Zealand White rabbits (2.1 ± 0.2 kg,
506 Charles River) – the most relevant small animal model for cardiac arrhythmia research[48] – and
507 were conducted in accordance with the ethical guidelines of the Canadian Council on Animal Care
508 as well as the German legislation for animal welfare, with protocols approved by the Dalhousie
509 University Committee for Laboratory Animals, or by the local Institutional Animal Care and Use
510 Committee at the University of Freiburg (Regierungspräsidium Freiburg, X-16/10R). Details have
511 been reported following the Minimum Information about a Cardiac Electrophysiology Experiment
512 (MICEE) reporting standard.[49]

513 **Cell isolation.** Animals were euthanised by ear vein injection of pentobarbital (140 mg/kg) and
514 heparin (1,500 units/kg, Sigma-Aldrich), followed by rapid excision of the heart, aortic
515 cannulation, and Langendorff perfusion (20 mL/min) with 37 °C modified Tyrode (NT) solution
516 (containing, in mM: 120 NaCl, 4.7 KCl, 1 $MgCl_2$, 1.8 $CaCl_2$, 10 glucose, 10 HEPES [Sigma-
517 Aldrich], with pH adjusted to 7.40 ± 0.05 with NaOH and an osmolality of 300 ± 5 mOsm/L)
518 bubbled with 100 % oxygen. After a rest period of 15 min, the perfusate was switched to calcium
519 (Ca^{2+})-free cardioplegic solution for 5 min (containing, in mM: 117 NaCl, 10 KCl, 1 $MgCl_2$, 10
520 creatine, 20 taurine, 5 adenosine, 2 L-carnitine, 10 glucose, 10 HEPES [Sigma-Aldrich], with pH
521 adjusted to 7.40 ± 0.05 with NaOH and an osmolality of 300 ± 5 mOsm/L), with an addition of
522 0.018 mM EGTA (Sigma-Aldrich). The perfusate was then switched to digestion solution,
523 comprised of Ca^{2+}-free solution with the addition of 200 U/mL Collagenase II (Worthington
524 Biochemical Corporation), 0.06 mg/mL Protease XIV (from *Streptomyces griseus*, Sigma
525 Aldrich), and 100 μM $CaCl_2$. After 5 min, the perfusion rate was reduced to 15 mL/min until the
526 heart became flaccid and jelly-like (~10-12 min). The left ventricular free wall was removed and

527 placed into 50 mL of stop solution, comprised of the Ca^{2+}-free cardioplegic solution described
528 above without EGTA, but with an addition of 0.5 % bovine serum albumin (Sigma Aldrich) and
529 100 μM $CaCl_2$. The tissue was agitated, the solution filtered through a 300 μm pore nylon mesh,
530 the tissue returned to fresh stop solution and re-agitated, and the solution filtered in duplicate. The
531 cell-containing filtered solution was divided into 2 mL microcentrifuge tubes and maintained at
532 room temperature.

533 **Carbon fibre method.** Cells were stretched using the carbon fibre method, adapted from previous
534 work.[19] Briefly, single carbon fibres (12-14 μm in diameter,) were mounted with cyanoacrylate
535 adhesive into a pair of borosilicate glass capillaries, pulled from glass tubes (1.12 mm
536 inner / 2 mm outer diameter, World Precision Instruments) and bent at 30 ° to allow near-parallel
537 alignment of the fibres with the bottom of the experimental chamber. Carbon fibres were trimmed
538 to a length of either 1.2 mm or 0.6 mm from the end of the glass capillary and used in combination
539 so that one fibre was relatively compliant and the other relatively stiff. Each carbon fibre-
540 containing capillary was mounted in a microelectrode holder (MEH820, World Precision
541 Instruments), coupled to a three-axis water hydraulic micromanipulator (MHW-103, Narishige)
542 on top of a linear piezo-electric translator (PZT, P-621.1CD, Physik Instrumente). The carbon fibre
543 position was controlled by a piezo amplifier / servo controller (E-665.CR, Physik Instrumente),
544 driven by a voltage signal generated from a data acquisition (DAQ) device (USB-6361; National
545 Instruments) and custom-written routines in LabVIEW (National Instruments). Prior to use on CM,
546 carbon fibre stiffness was calibrated by pressing a fibre against a force transducer system (406A,
547 Aurora Scientific), measuring the force for given displacements of the PZT, and fitting the data by
548 linear regression to the formula: stiffness = force / carbon fibre bending (where bending = PZT
549 displacement). This allowed measurement of passive and active forces of CM by tracking carbon

550 fibre bending (monitoring fibre tips and prescribing PZT position; described below). Force was
551 calculated as: force = stiffness × (change in distance between carbon fibre tips - change in distance
552 between PZT positions). Stress was assessed by dividing force by the stretched cross-sectional
553 area (CSA) of the CM, determined by assuming that the cross section is an ellipse with CSA =
554 $\pi \times$ (cell width / 2) $\times$ (cell thickness / 2), where cell thickness is assumed to be = width / 3.[50]

555 **Single cell stretch.** Before use, half of the supernatant from the cell-containing microcentrifuge
556 tube was removed and replaced by room temperature NT for 10 min (so that cells were exposed to
557 50 % of normal extracellular Ca^{2+} concentration), after which all of the supernatant was removed
558 and replaced by NT. A drop of cell-containing solution was added to an imaging chamber (RC-
559 27NE2, Warner Instruments) containing 1 mL of NT maintained at 35 °C by a temperature
560 controller (TC-344C, Warner Instruments) and mounted on an inverted fluorescence microscope
561 (IX-73, Olympus) with a 40× objective (UPLFLN40X, Olympus). The surface of the coverslip on
562 the bottom of the chamber was coated with poly-2-hydroxyethyl methacrylate (poly-HEMA,
563 Sigma-Aldrich) to prevent cell adhesion. Once the cells had settled, 1 Hz biphasic electrical field
564 stimulation (100 mA, 2 ms square pulse duration; SIU-102, Warner Instruments) was commenced
565 and homogeneously contracting, rod-shaped CM with clear striations and well-defined membranes
566 lacking signs of blebbing were selected. Electrical stimulation was stopped, and one long and one
567 short carbon fibre were positioned above either end of a CM and gently lowered onto the cell
568 surface using the hydraulic micromanipulators. Adhesion of the CM to carbon fibres was
569 confirmed by raising the cell off the coverslip. Once cell attachment was established, electrical
570 stimulation was recommenced, and cells contracted against the mechanical afterload imposed by
571 carbon fibres for ~1-2 min, which improved cell adhesion. Cells were then superfused at
572 2.1 mL/min through an inline heater (SF-28, Warner Instruments) with either NT or pinacidil-

573 containing solution (50 μM, to activate ATP-sensitive potassium, K_{ATP}, channels) for 5 min. To
574 approximate stretch of ischaemically weakened myocardium during acute regional ischaemia,[51-55]
575 transient stretch (20 μm PZT displacement, applied and removed at a rate of 0.7 μm/ms) was
576 applied (Fig. 2a). Stretch was timed from the electrical stimulus, to occur at two times during the
577 AP, with 10 s between each stretch: first during mid-diastole (600 ms delay after an electrical
578 stimulus), and then during the vulnerable period of the repolarisation-relaxation coupling interval
579 (VP_{RRC}; 150 ms delay, so that a majority of stretches – whose duration increased with greater PZT
580 displacement – would occur within the VP_{RRC}, based on the timing measured by simultaneous
581 voltage-Ca^{2+} imaging; described below). These two differentially timed stretches were then
582 duplicated, such that there was a total of four stretches at each magnitude of PZT displacement.
583 This protocol was repeated with increasing magnitudes of PZT displacement (30 and 40 μm) to
584 generate a range of stretch-induced changes in sarcomere length within a cell (30 s between
585 repetitions, for a total of 12 stretches; Fig. 2b).

586 **Assessment of stretch effects.** Throughout the protocol, sarcomere length, PZT location, and
587 carbon fibre tip positions were monitored and recorded at 240 Hz (Myocyte Contractility
588 Recording System, IonOptix). From this, CM contractile function (diastolic sarcomere length, and
589 maximum rate and percent sarcomere shortening), as well as characteristics of cell stretch (percent
590 sarcomere stretch, peak sarcomere length, and maximum applied stress) were obtained.
591 Arrhythmic activity was assessed from sarcomere length measurements, which revealed stretch-
592 induced premature contractions (defined as 1 or 2 unstimulated contractions after stretch), or other
593 self-sustained arrhythmic activity (including refractoriness, resulting in single or multiple missed
594 beats, or sustained activity that either spontaneously resolved, or was terminated by an additional
595 stretch). Examples of each type of stretch-induced arrhythmia are provided in Fig. 2. Any stretch

596 that resulted in carbon fibre detachment, or a sustained arrhythmia that did not spontaneously
597 resolve or could not be terminated by a maximum of two additional stretch applications was
598 excluded (< 1 % of all cells).

599 **Pharmacological interventions.** Pharmacological agents dissolved as stock solutions in distilled
600 water, dimethyl sulfoxide (DMSO), or ethanol, as appropriate, were added to the perfusate and
601 continuously perfused for 5 min before any recordings. Agents included: BAPTA-AM (1 μM from
602 a stock concentration of 10 mM in DMSO, to buffer cytosolic Ca^{2+}, with the concentration
603 determined in preliminary experiments by titrating to a value that caused a ~ 10 % decrease in
604 percent sarcomere shortening during contraction, Abcam), dantrolene (1 μM from a stock
605 concentration of 5 mM in DMSO, to stabilise ryanodine receptors, Abcam), streptomycin (50 μM
606 from a stock concentration of 15 mM in distilled water, to non-specifically block mechano-
607 sensitive channels, Sigma-Aldrich), HC-030031 (10 μM from a stock concentration of 50 mM in
608 DMSO, to block TRPA1 channels, Abcam), allyl isothiocyanate (AITC, 10 μM from a stock
609 concentration of 1 M in DMSO, to activate TRPA1 channels, Sigma-Aldrich), and paclitaxel
610 (10 μM from a stock concentration of 10 mM in DMSO, to increase the polymerisation and
611 stabilisation of microtubules, Abcam). For BAPTA-AM, HC-030031, and paclitaxel, cells were
612 incubated for 20, 30, or 90 min respectively, after introduction to NT but prior to superfusion.

613 **Dual parametric voltage-Ca^{2+} fluorescence imaging.** The Ca^{2+}-sensitive dye Fluo-5F, AM
614 (5 μM from a stock concentration of 1 mM in DMSO, ThermoFisher Scientific) and Pluronic F-
615 127 (0.02 % from a stock concentration of 20 % in DMSO, Biotium) were added to the cell-
616 containing microcentrifuge tube during cellular suspension in the 50 % Ca^{2+} solution, and cells
617 were incubated in the dark for 20 min. The supernatant was then replaced with fresh NT, the
618 voltage-sensitive dye di-4-ANBDQPQ (20 μM from a stock concentration of 28.8 mM in ethanol,

619 University of Connecticut Health Centre) was added to the tube, and the cells were incubated in
620 the dark for 14 min. The supernatant was again replaced with fresh NT, probenecid (1 mM from a
621 stock concentration of 250 mM in distilled water, Sigma-Aldrich) was added to the tube, and the
622 cells were from there on maintained in the dark at room temperature. For imaging, the solution
623 containing dye-loaded cells was gently agitated with a transfer pipette and a drop of solution was
624 added to 1 mL of NT in the imaging chamber. Carbon fibres were attached to a cell as described
625 above (carbon fibres reduced motion artefact associated with cell translocation in the vertical plane
626 during contractions, allowing measurements to be made without an excitation-contraction
627 uncoupler). Fluorescence was excited by light from a mercury lamp (U-HGLGPS, Olympus),
628 passed through a 466 / 40 nm bandpass filter (FF01-466/40, Semrock) and reflected onto the
629 sample by a 495 nm dichroic mirror (FF495-Di03, Semrock). For simultaneous measurement of
630 trans-membrane voltage and cytosolic 'free' Ca^{2+} concentration ($[Ca^{2+}]_i$), each fluorescent signal
631 was projected onto one-half of a 128 × 128-pixel, 16-bit electron-multiplying charge-coupled
632 device (EMCCD) camera sensor (iXon3, Andor Technology) using an emission image splitter
633 (Optosplit II; Cairn Research), and recorded at 500 fps with 2 ms exposure time and maximum
634 electron-multiplying gain. The two signals were split with a 685 nm dichroic mirror (FF685-Di02,
635 Semrock) and Fluo-5F emission was collected with a 525 / 50 nm bandpass filter (FF03-525 / 50,
636 Semrock) and di-4-ANBDQPQ emission with a 700 nm long-pass filter (HQ700lp; Chroma
637 Technology). A schematic of the imaging setup is provided in Fig. 1a.

638 Analysis of voltage and $[Ca^{2+}]_i$ signals was performed using custom routines in Matlab
639 (R2018a, MathWorks). Fluorescence for each signal was averaged over the entire cell, a temporal
640 filter (50 Hz low-pass Butterworth) was applied, and effects of bleaching were corrected by fitting
641 the resulting signal with a second-order polynomial and subtracting the result. From the corrected

642 signals, time to 50 % or 80 % recovery of the action potential (action potential duration, APD_{50} or
643 APD_{80}) or the $[Ca^{2+}]_i$ transient ($[Ca^{2+}]_i$ transient duration, $CaTD_{50}$ or $CaTD_{80}$) were averaged over
644 3 consecutive cardiac cycles. The VP_{RRC} was calculated as the difference between $CaTD_{80}$ and
645 APD_{50}, plus the difference between the timing of the action potential and $[Ca^{2+}]_i$ transient
646 upstrokes, measured at the point of maximum upstroke velocity for each signal (excitation-
647 contraction coupling time, ECC, see Fig. 1b, d): $VP_{RRC} = (CaTD_{80} - APD_{50}) + ECC$.

648 **Ratiometric $[Ca^{2+}]_i$ fluorescence imaging.** Imaging of $[Ca^{2+}]_i$ levels was performed using the
649 ratiometric Ca^{2+}-sensitive dye Fura Red, AM ($K_d \approx 400$ nM, AAT Bioquest). Cells were incubated
650 in the dark for 20 min with 5 μM of the dye (from a stock concentration of 1 mM in DMSO),
651 0.02 % Pluronic F-127, and 1 mM probenecid. Fluorescence was excited by alternating light pulses
652 from two white light-emitting diodes (CFT-90-W; Luminus Devices), one with a 420 / 10 nm
653 bandpass filter (FF01-420 / 10, Semrock) and the other with a 531 / 22 nm bandpass filter (FF02-
654 531/22, Semrock), which were combined into the microscope excitation light path with a 455 nm
655 dichroic mirror (AT455dc, Chroma Technology) and reflected onto the sample by a 562 nm
656 dichroic mirror (T562lpxr, Chroma Technology). Fluorescence was measured through a
657 632 / 60 nm bandpass filter (AT635 / 60m, Chroma Technology) with the EMCCD camera at
658 500 fps with 2 ms exposure time and maximum electron-multiplying gain. Light pulses and camera
659 frame acquisition were synchronised with a custom control box (provided by Dr. Ilija Uzelac,
660 Georgia Institute of Technology) so that alternating frames corresponded to the signal generated
661 by each of the two excitation wavelengths.[56]

662 Analysis of $[Ca^{2+}]_i$ was performed using custom routines in Matlab. Fluorescence was averaged
663 over the entire cell and a temporal filter (50 Hz low-pass Butterworth) was applied. The two Ca^{2+}
664 signal emissions were separated, and the ratio of the signals was calculated. Any remaining

665 bleaching was corrected by fitting the resulting signal with a second-order polynomial and
666 subtracting the result. From the corrected signals, the minimum value for each cardiac cycle
667 (representing a relative measurement of diastolic $[Ca^{2+}]_i$) was established and averaged over 3
668 consecutive cardiac cycles.

669 **Cell immunofluorescence.** Coverslips (22 mm round; VWR) were coated with laminin
670 (100 μg/mL from Engelbreth-Holm-Swarm murine sarcoma basement membrane diluted in PBS,
671 Sigma-Aldrich) and stored in a 12-well plate (VWR). Isolated CM in NT were added to each well
672 and maintained at room temperature for 3 hours to seed. In half of the wells, paclitaxel (10 μM)
673 was added for the final 90 min. Cells were then fixed by removing the NT and submerging the
674 cover slips in ice cold methanol and incubating for 7 min at -20 ºC. Methanol was removed and
675 cover slips were rinsed 5 times with phosphate buffered saline (PBS, Sigma-Aldrich) to remove
676 excess methanol. Cover slips were stored in PBS until staining.

677 For staining, coverslips were bathed in blocking solution (5 % BSA in PBS, Sigma-Aldrich) at
678 room temperature for 1 hour. Coverslips were then transferred to a custom-built humidity chamber
679 (a glass Petri dish lined with a PBS-soaked piece of tissue placed on upside down on top of a piece
680 of Parafilm). Diluted primary antibody (100 μL of 1:200 rat anti-rabbit a-tubulin, Clone YL1 / 2,
681 Invitrogen) was pipetted onto the Parafilm and the coverslips were placed cell-side down on top
682 of the solution and incubated at 4 ºC for 1 hour. Coverslips were subsequently washed in
683 quadruplicate (5 min each) with PBS and diluted secondary antibody (1:500 goat anti-rat IgG
684 Alexa Fluor 488 conjugate, Invitrogen) was applied as above. Following secondary antibody
685 staining, coverslips were mounted cell-side down to glass slides with mounting medium (ProLong
686 Glass Antifade Mountant with NucBlue Stain, ThermoFisher).

687 Imaging of fixed and stained CM was performed on an inverted confocal microscope system
688 (TCS SP8, Leica) with a 40x oil immersion, 1.3 NA objective (HC Plan APOCHROMAT CS2,
689 Leica) and Lightning deconvolution software to obtain super-resolution images. Samples were
690 illuminated with a 488 nm solid state laser at 1.2 % intensity and the photomultiplier tube (PMT)
691 detectors were set to collect between 503-577 nm. A z-stack of 3 images, spaced at 1.5 μm, was
692 obtained. Maximum projections were generated using Leica LAS X 3D viewer software. Images
693 were then analysed in a blinded fashion, using custom software in Fiji (kindly shared by Drs
694 Matthew Caporizzo and Benjamin Prosser, Department of Physiology, University of Pennsylvania
695 Perelman School of Medicine, Philadelphia, USA) to determine microtubule density, calculated as
696 the fraction of cell area.[57] Briefly, cells were manually traced and a threshold for microtubule
697 positive pixels was determined from a background region within the cell with no visible
698 microtubule fluorescence. This was used to generate a binary image of the cell to calculate the
699 microtubule positive fraction of the total cell area.

700 **Tissue Western blotting.** Boiled samples of left ventricular free wall (20 μg) were separated (4 %
701 stacking gel) and resolved *via* 7.5 % sodium dodecyl sulfate-polyacrylamide gel electrophoresis
702 (Mini-PROTEAN SDS-PAGE, BioRad). Samples were loaded alongside 10 μL protein ladder
703 (Precision Plus Protein Standards Kaleidoscope ladder, BioRad). Self-cast gels (Mini-PROTEAN,
704 BioRad) were run on ice at 90 V for 30 min and then at 120 V until the dye front migrated to the
705 opposite edge of the gel on ice in 1X Tris / Glycine / SDS electrophoresis buffer (BioRad).
706 Samples were wet-transferred to nitrocellulose (0.2 μm, BioRad) at 100 V for 1.5 hours buried in
707 ice. Membranes were briefly rinsed in double-distilled water and equal protein transfer was
708 confirmed by incubating the membranes in stain (Pierce Reversible Memcode Stain, Thermo
709 Scientific) for 5 min. The stained blot was labelled and imaged (ChemiDoc MP Imaging System,

710 BioRad) before removing the stain (Pierce Stain Eraser, Thermo Scientific). Membranes were then
711 blocked in 5 % skim-milk in 1X Tris-Buffered-Saline-Tween 20 (TBS-T, Sigma-Aldrich) for 60
712 min. Membranes were subsequently incubated overnight at 4 ºC with primary antibodies (1:2,000
713 monoclonal mouse anti-TRPA1 antibody, Sigma-Aldrich, and 1:3,000 MF20 mouse anti-myosin
714 heavy chain antibody, Hybridoma Bank), diluted in 1 % skim-milk in TBS-T with sodium azide.
715 Next, blots were incubated with secondary antibody (1:4000 horseradish peroxidase HRP-
716 conjugated anti-mouse produced in goat, Jackson Labs) for 1 hour in 5 % skim-milk at room
717 temperature. Immunoreactivity was then measured (Clarity Western Enhanced
718 Chemiluminescence Substrate, with a ChemiDoc MP Imaging System, BioRad). Membranes were
719 stripped by incubation in 25 mL 0.5 M Tris-HCl / SDS buffer supplemented with 125 µL 2-
720 mercaptoethanol (Sigma-Aldrich) for 1 hour and re-probed.

721 **Patch-clamp current recordings.** Cells for patch clamp experiments were isolated from
722 ventricular slices according to a previously published protocol.[58] Briefly, animals were
723 anaesthetised by intramuscular injection of esketamine hydrochloride (0.5 mL/kg) and 2 %
724 xylazine hydrochloride (0.2 mL/kg). Under sedation, an anaesthetic mixture of sodium-heparin
725 (1,000 units/mL) and esketamine hydrochloride (25 mg/mL) were injected intravenously.
726 Euthanasia was induced by intravenous injection of sodium-thiopental (25 mg/mL) until apnoea.
727 The heart was then swiftly excised, cannulated, and Langendorff perfused (20 mL/min) for 2 min
728 with 37 °C modified NT solution (containing, in mM: 137 NaCl, 4 KCl, 10 $MgCl_2$, 1.8 $CaCl_2$, 10
729 glucose, 10 HEPES, 10 creatine, 20 taurine, 5 adenosine, 2 L-carnitine; with pH adjusted to
730 7.30 ± 0.05 with NaOH) bubbled with 100 % oxygen, followed by 2 min with 37 °C cutting
731 solution (containing, in mM: 138 NaCl, 5.4 KCl, 0.33 NaH_2PO_4; 2.0 $MgCl_2$, 0.5 $CaCl_2$, 10 HEPES,
732 30 2,3-butanedione 2-monoxime (BDM); with pH adjusted to 7.30 ± 0.05 with NaOH) bubbled

733 with 100 % oxygen. The left ventricular free wall was cut into approximately 0.8 mm x 0.8 mm
734 wide transmural tissue chunks, embedded in 4 % low melting point agarose dissolved in cutting
735 solution. Left ventricular blocks were cut into 300 µm thick live tissue slices, using a vibrating
736 microtome (7000 smz-2, Campden Instruments Ltd) with stainless-steel blades (7550-1-SS,
737 Campden Instruments Ltd) at 4 °C, with 60 Hz horizontal blade displacements of 1.5 mm, at a
738 blade progression velocity of 0.05 mm/s (Z-deflection values were below 1 µm). Slices were
739 stored at 4 °C in cutting solution until digestion.

740 Slices were digested at 37 °C in Petri dishes (Ø 35 mm) placed on a heated orbital shaker (50-
741 65 rpm). Slices were washed three times (1 min for each wash) with the solution used for cell
742 isolation, but without digestive enzymes (containing, in mM: 100 NaCl, 15 KCl, 2.5 KH_2PO_4, 2
743 $MgCl_2$, 10 glucose, 10 HEPES, 20 taurine, 20 L-glutamic acid monopotassium salt, 30 BDM; with
744 2 mg/mL bovine serum albumin; pH adjusted to 7.30 ± 0.05 with NaOH). Slices were then digested
745 for 12 min by including proteinase type XXIV (0.5 mg/mL; Sigma-Aldrich) to the cell isolation
746 solution mentioned above, followed by three more washes. Digestion was continued by adding
747 200 µL of Liberase™ TL Research Grade (0.25 mg/mL; Hoffmann-La Roche) per 2 mL of cell
748 isolation solution, supplemented with 5 µM $CaCl_2$. When slices started to show a corrugated
749 appearance (~ 25 - 50 min), they were washed three times with the solution used for cell isolation,
750 without enzymes but containing 10 mg/mL bovine serum albumin, and mechanically dissociated
751 using forceps and gentle pipetting with Pasteur pipettes. The Ca^{2+} concentration was increased in
752 a stepwise fashion every 5 min (to 5 µM, 12 µM, 20 µM, 42 µM, 84 µM, 162 µM, 266 µM,
753 466 µM, 827 µM, and 1 mM), during which time BDM was gradually decreased to a final
754 concentration of 13 mM. Cells were filtered through a 1-mm-pore nylon mesh and allowed to settle
755 in a conical centrifuge tube for 15 - 20 min. The supernatant was removed and replaced by

756 modified NT. Quality of the preparation was assessed by the percentage of rod-shaped cells, the
757 response to electrical pacing, and the resting sarcomere length. Cells with irregular / unclear
758 sarcolemma, blebs, or unclear striations were rejected.

759 Sarcolemmal ion channel activity was recorded at room temperature (21 ± 2 °C) using the
760 patch-clamp technique with a holding potential of +40 mV. Recordings were obtained in cell-
761 attached configuration using a patch-clamp amplifier (Axopatch 200B, Axon Instruments) and a
762 digitiser interface (Axon Digidata 1440A, Axon Instruments). Fire-polished soda-lime glass
763 capillaries (1.15 ± 0.05 mm inner / 1.55 ± 0.05 mm outer diameter; VITREX Medical A/S) were
764 pulled using a two-stage pipette-puller (PC-10, Narishige) to create the micropipettes required for
765 patch-clamping. Average pipette resistance was 1.36 ± 0.10 MΩ. Currents were acquired at
766 20 kHz sampling rate (interval 50 µs), and low-pass filtered at 1 kHz. Currents were analysed with
767 pCLAMP 10.6 software (Axon Instruments). The bath solution contained (in mM): 155 KCl, 3
768 $MgCl_2$, 5 EGTA, 10 HEPES (Sigma-Aldrich), with pH adjusted to 7.2 ± 0.05 using KOH and an
769 osmolality of 310 ± 5 mOsm/L. The solution was stored at room temperature. Pipette solution for
770 cell-attached recordings contained (in mM): 150 NaCl, 5 KCl, 10 HEPES, 2 $CaCl_2$ with pH
771 adjusted to 7.4 ± 0.05 using NaOH and an osmolality of 300 ± 5 mOsm/L. The pipette solution
772 also contained 10 mM tetraethylammonium chloride (TEA), 5 mM 4-aminopyridine, and 10 mM
773 glibenclamide to inhibit potentially contaminating potassium channels. These ionic conditions
774 were used previously to assess cation non-selective channels.[59] AITC was added to the bath
775 solution before use and perfused *via* a local perfusion system. Flow rate was adapted by adjusting
776 the height of reservoirs for gravity-fed flow to 1 mL/min. Recordings were analysed in Clampfit
777 10.6. Average current was calculated over at least 10 s for each condition.

Statistics. Statistics were performed using Prism 9 (GraphPad). Differences in arrhythmia incidence were assessed using chi-square contingency tables and Fisher's exact test. Data was first tested for normality, then differences between group means were assessed by two-tailed, paired or unpaired Student's t-test (for normally distributed data), Wilcoxon matched-pairs (paired) or Mann-Whitney (unpaired) test (for data that was not normally distributed), one-way ANOVA with Tukey *post-hoc* tests (for normally distributed data), or Kruskal-Wallis with Dunn's multiple comparisons test (for data that was not normally distributed), where appropriate. The relevant test is indicated in the figure captions. A p-value of < 0.05 was considered indicative of a significant difference between observed parameters. Figures indicate the number of replicates used in each experiment (N = rabbit hearts / group, n = cells / group, m = stretch stimuli applied / analysed).

Data availability. The datasets obtained and analysed in the current study are available from the corresponding author upon reasonable request.

Code availability. All custom computer source code used in this study is available from the corresponding author upon reasonable request.

792 **METHODS REFERENCES**

793 48. Clauss, S. *et al*. Animal models of arrhythmia: classic electrophysiology to genetically
794 modified large animals. *Nat. Rev. Cardiol*. **16**, 457-75 (2019).
795 49. Quinn, T. A. *et al*. Minimum Information about a Cardiac Electrophysiology Experiment
796 (MICEE): standardised reporting for model reproducibility, interoperability, and data sharing.
797 *Prog. Biophys. Mol. Bio.* **107**, 4-10 (2011).
798 50. Peyronnet, R. *et al*. Load-dependent effects of apelin on murine cardiomyocytes. *Prog.*
799 *Biophys. Mol. Biol.* **130**, 333-43 (2017).
800 51. Gallagher, K. P., Gerren, R. A., Choy M., Stirling M. C. & Dysko R. C. Subendocardial
801 segment length shortening at lateral margins of ischaemic myocardium in dogs. *Am. J.*
802 *Physiol*. **253**, H826-37 (1987).
803 52. Prinzen, F. W., Arts, T., Hoeks, A. P. G. & Reneman, R. S. Discrepancies between myocardial
804 blood flow and fiber shortening in the ischaemic border zone as assessed with video mapping
805 of epicardial deformation. *Pflügers Archiv*. **415**, 220-9 (1989).
806 53. Sakai, K., Watanabe, K., Millard, R. W. Defining the mechanical border zone: a study in the
807 pig heart. *Am. J. Physiol*. **249**, H88-94 (1985).
808 54. Theroux, P., Franklin, D., Ross, J., Kemper, W. S. Regional myocardial function during acute
809 coronary artery occlusion and its modification by pharmacologic agents in the dog. *Circ. Res*.
810 **35**, 896-908 (1974).
811 55. Rodriguez, F. et al. Alterations in transmural strains adjacent to ischemic myocardium during
812 acute midcircumflex occlusion. *J. Thorac. Cardiovasc. Surg*. **129**, 791-803 (2005).

813 56. Lee, P., Bollensdorff, C., Quinn, T. A., Wuskell, J. P., Loew, L. M. & Kohl, P. Single-sensor
814 system for spatially-resolved, continuous and multi-parametric optical mapping of cardiac
815 tissue. *Heart Rhythm*. **8**, 1482-91 (2011).
816 57. Chen, C. Y., Caporizzo, M. A., Bedi, K., Vite, A., Bogush, A. I., Robison, P., Heffler, J. G.,
817 Salomon, A. K., Kelly, N. A., Babu, A., Morley, M. P., Margulies, K. B., Prosser, B. L.
818 Suppression of detyrosinated microtubules improves cardiomyocyte function in human heart
819 failure. *Nat. Med*. **24**, 1225-33 (2018).
820 58. Fiegle, D. J., Volk, T., Seidel, T. Isolation of human ventricular cardiomyocytes from
821 vibratome-cut myocardial slices. *J. Vis. Exp.* **159**, e61167 (2020).
822 59. Peyronnet, R. *et al*. Piezo1-dependent stretch-activated channels are inhibited by Polycystin-
823 2 in renal tubular epithelial cells. *EMBO Rep*. **14**, 1143-8 (2013).
824

825 **STATEMENTS**

826 **Acknowledgements.** We thank Gentaro Iribe (Asahikawa Medical University, Asahikawa, Japan)
827 and Keiko Kaihara (Okayama University, Okayama, Japan) for technical assistance with cell
828 stretch. Carbon fibres were a gift from Jean-Yves LeGuennec. This work was supported by the
829 Canadian Institutes of Health Research (MOP 342562 to T.A.Q.); by the Natural Sciences and
830 Engineering Research Council of Canada (RGPIN-2016-04879 to T.A.Q.); by the Dalhousie
831 Medical Research Foundation (T.A.Q.); by the Canadian Foundation for Innovation (32962 to
832 T.A.Q.); and by the Heart and Stroke Foundation of Canada through a National New Investigator
833 award (T.A.Q.). B.A.C., J.G., R.P. and P.K. are members of the German Research Foundation
834 Collaborative Research Centre SFB1425 (DFG #422681845).

835 **Author contributions.** B.A.C. and T.A.Q. designed the study, interpreted the data, and wrote the
836 manuscript; B.A.C. performed and analysed the cell stretch, stiffness, and fluorescence imaging
837 experiments, and isolated cells for the immunofluorescence experiments; M.R.S. contributed to
838 experimental design and setup; J.G. isolated cells for the patch-clamp experiments; R.P. performed
839 and analysed the patch-clamp experiments; M.S.C. performed and analysed the Western blotting
840 experiments; and J.J.B. and E.A.D. performed and analysed the immunofluorescence experiments.
841 P.K. contributed to the intellectual content of the research and revised the manuscript. All authors
842 read and approved the manuscript.

843 **Author information.** The authors declare no competing interests. Correspondence and request for
844 materials should be addressed to T.A.Q. (alex.quinn@dal.ca).

845

EXTENDED DATA

Extended Data Figure 1 | Mechanical characteristics of cell stretch. a, Percent sarcomere stretch, **b,** stretched sarcomere length, and **c,** maximum applied stress during acute diastolic stretch of rabbit isolated left ventricular cardiomyocytes exposed to Tyrode (NT, grey, left) or pinacidil (PIN, white, right, 50 μM, to activate ATP-sensitive potassium channels) with increasing levels of piezo-electric translator (PZT) displacement (20, 30, and 40 μm). Differences assessed by one-way ANOVA, with Tukey *post-hoc* tests for **a** and **b**, and by Kruskal-Wallis test for **c**. *$p < 0.05$, **$p < 0.01$, ***$p < 0.001$. N = rabbits / group, n = cells / group.

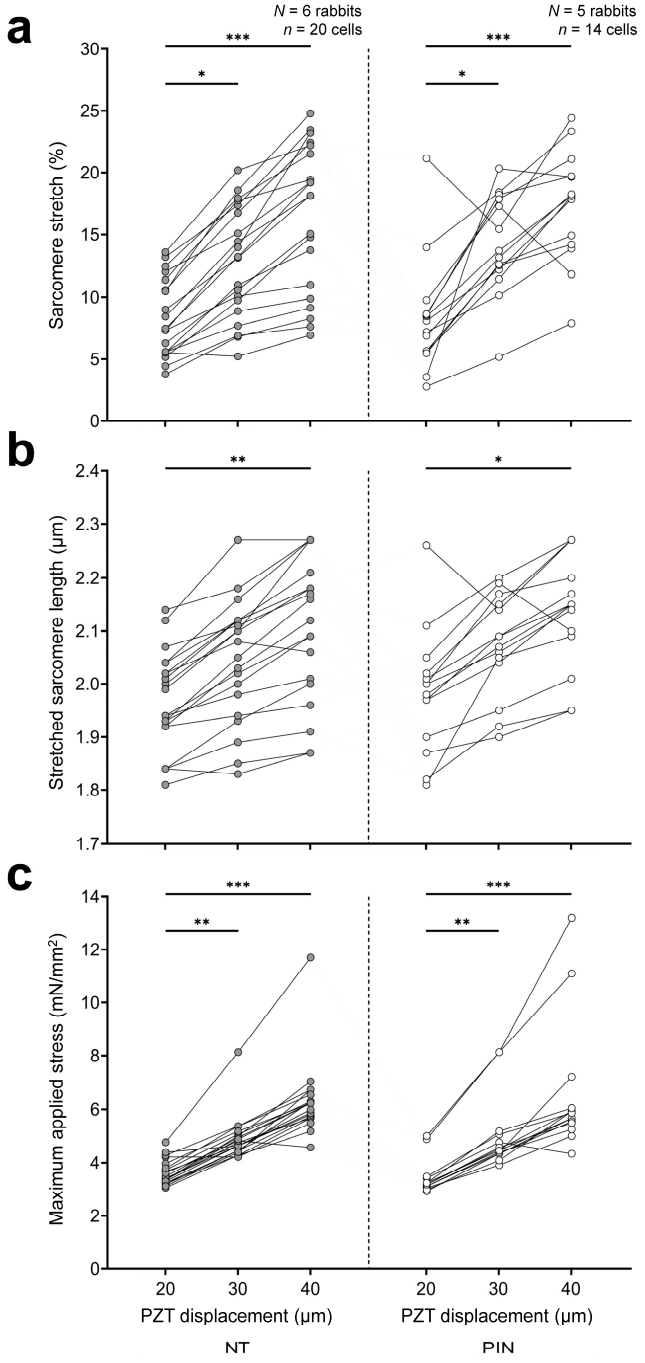

857 **Extended Data Figure 2 | Effect of stretch magnitude on the incidence of mechano-**
858 **arrhythmogenesis.** Incidence of premature contractions (blue) and other self-sustained
859 arrhythmic activity (shades of red) with rapid stretch at increasing levels of piezo-electric translator
860 (PZT) displacement in rabbit isolated left ventricular cardiomyocytes exposed to either Tyrode
861 (NT, left) or pinacidil (PIN, right, 50 μM, to activate ATP-sensitive potassium channels).
862 Differences assessed using chi-square contingency tables and Fisher's exact test. *$p < 0.05$. N =
863 rabbits / group, n = cells / group, m = stretch stimuli applied.
864

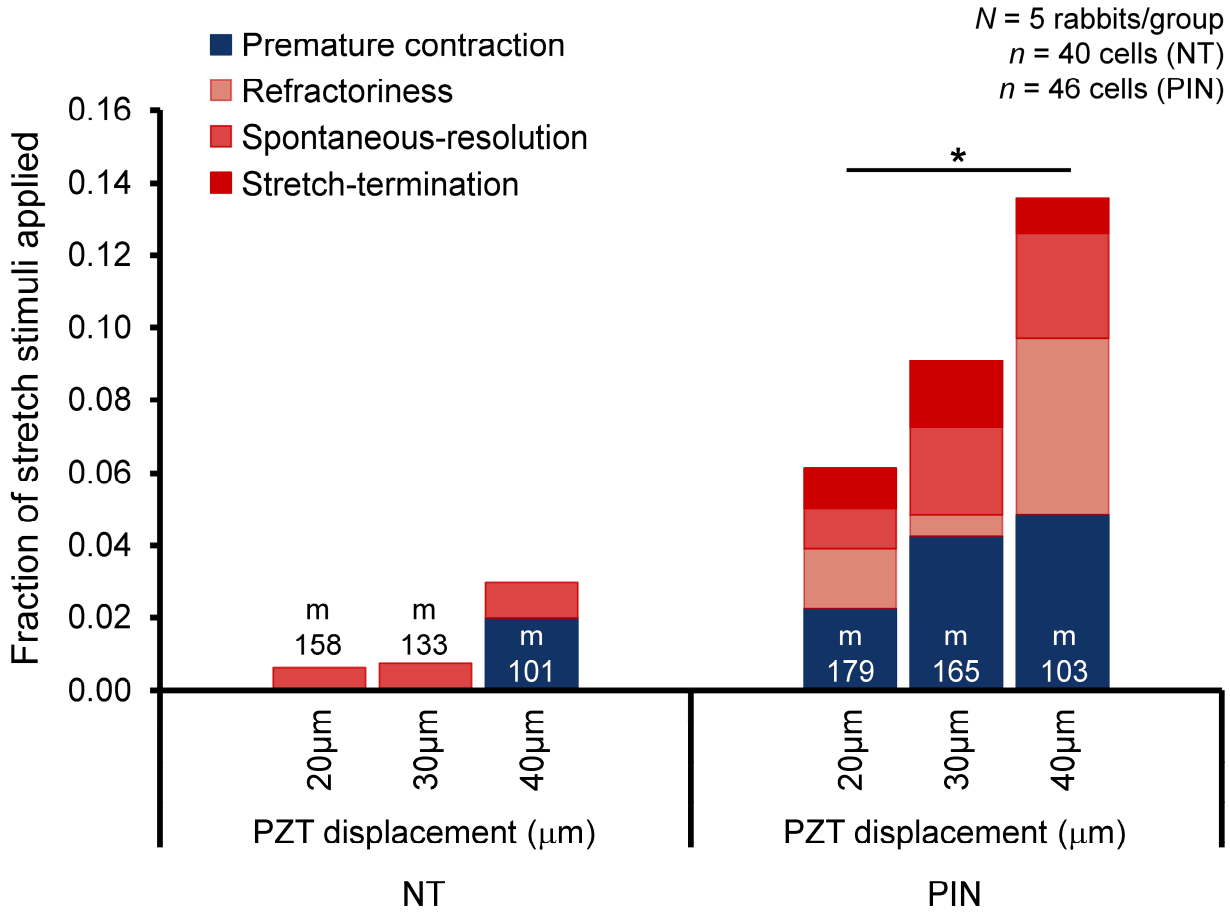

865
866

867 **Extended Data Figure 3 | Contractile function before and after stretch in control cells, and**
868 **in cells with pinacidil (PIN)-induced disruption of repolarisation-relaxation coupling (RRC).**
869 **a,** Diastolic sarcomere length and **b,** maximum rate and **c,** percent sarcomere shortening during
870 contraction of rabbit isolated left ventricular cardiomyocytes exposed to either Tyrode (NT, grey,
871 left) or PIN (white, right, 50 µM, to activate ATP-sensitive potassium channels) before (pre-
872 stretch) or after three successive diastolic stretch applications, generated by piezo-electric
873 translator (PZT) displacement (three stretch amplitudes applied were 20, 30 or 40 µm).
874 Measurements for each point averaged over 5 electrically paced contractions. Differences assessed
875 by one-way ANOVA, with Tukey *post-hoc* tests. *N* = rabbits / group, *n* = cells / group.
876

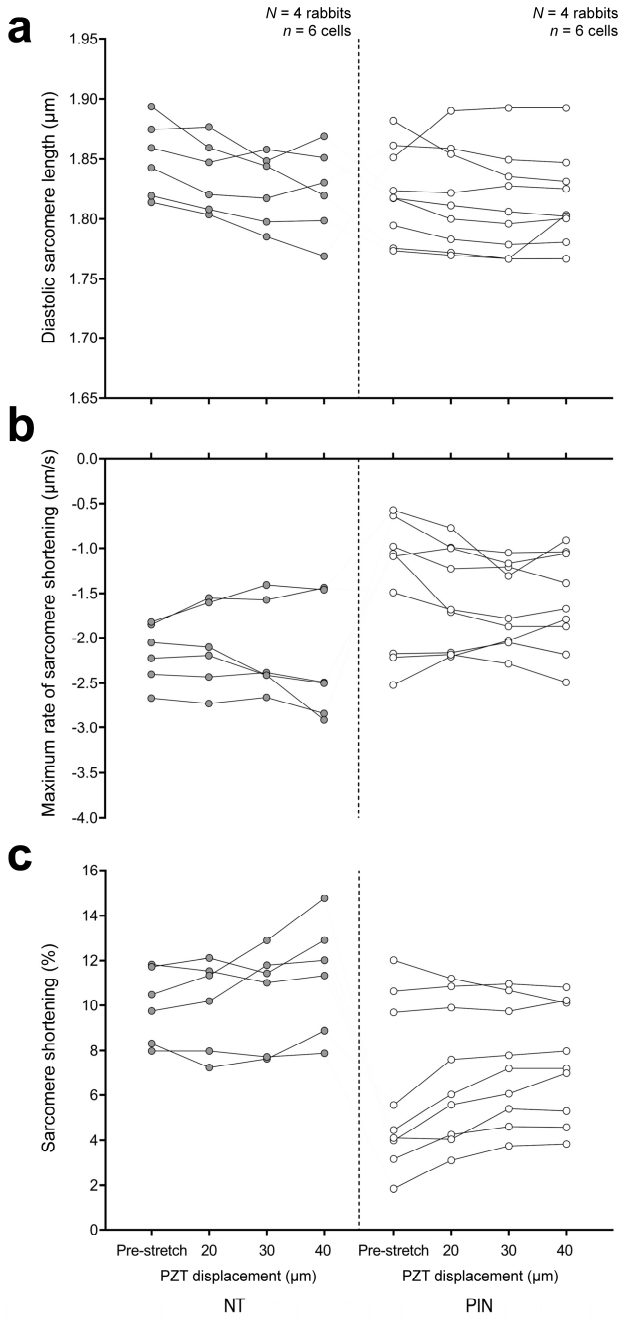

877

878 **Extended Data Figure 4 | Contractile function after termination of periods with sustained**
879 **arrhythmic activity. a,** Diastolic sarcomere length and **b,** maximum rate and **c,** percent sarcomere
880 shortening during contraction of rabbit isolated left ventricular cardiomyocytes in the presence of
881 pinacidil (50 µM, to activate ATP-sensitive potassium channels) before (green) and after (red)
882 termination of stretch-induced self-sustained arrhythmic activity. Measurements for each point
883 averaged over 5 electrically paced contractions. Differences assessed using two-tailed, paired
884 Student's t-test. *N* = rabbits, *n* = cells.
885

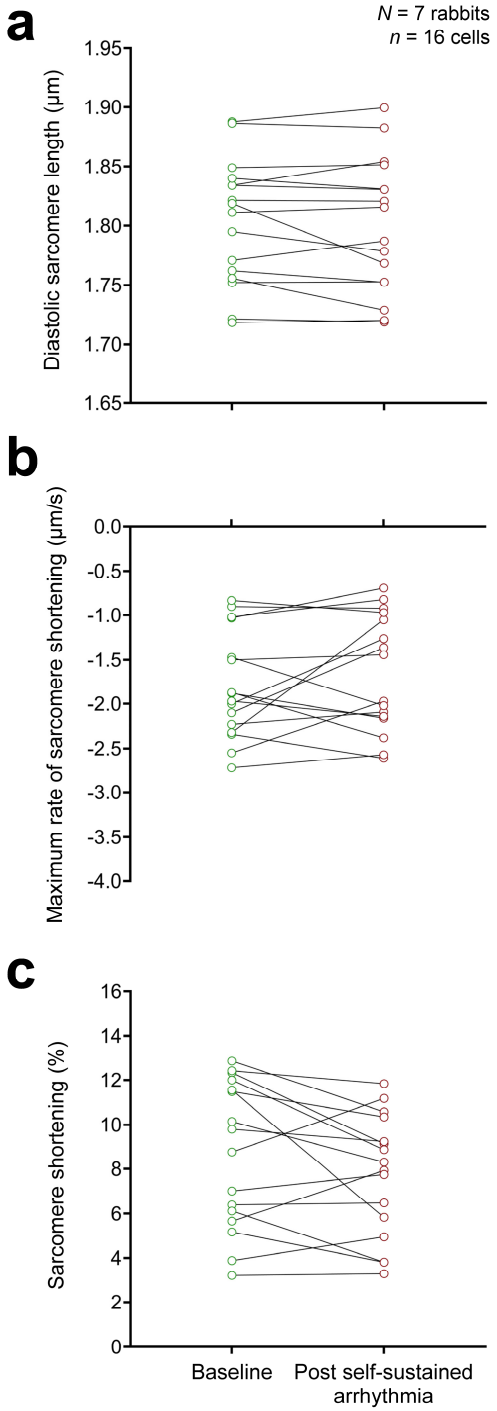

886

887 **Extended Data Figure 5 | Expression of transient receptor potential ankyrin 1 (TRPA1)**
888 **channels in rabbit left ventricular myocardium. a**, Western blot of TRPA1 and myosin heavy
889 chain (MF20) protein expression in rabbit left ventricular free wall tissue. **b**, Representative
890 recording of channel activation in response to allyl isothiocyanate (AITC, 50 μM, to activate
891 TRPA1 channels) in a cell-attached patch (holding potential +40 mV). **Inset**, Detail of channel
892 activation with visible single channel events. **c**, Quantification of AITC-induced current changes
893 (left) and comparison to time-matched same-batch control cells (right). Differences assessed with
894 two-tailed, paired Student's t-test. $^{**}p < 0.01$. Error bars represent standard error of the mean. *N*
895 = rabbits / group, *n* = cells / group.
896

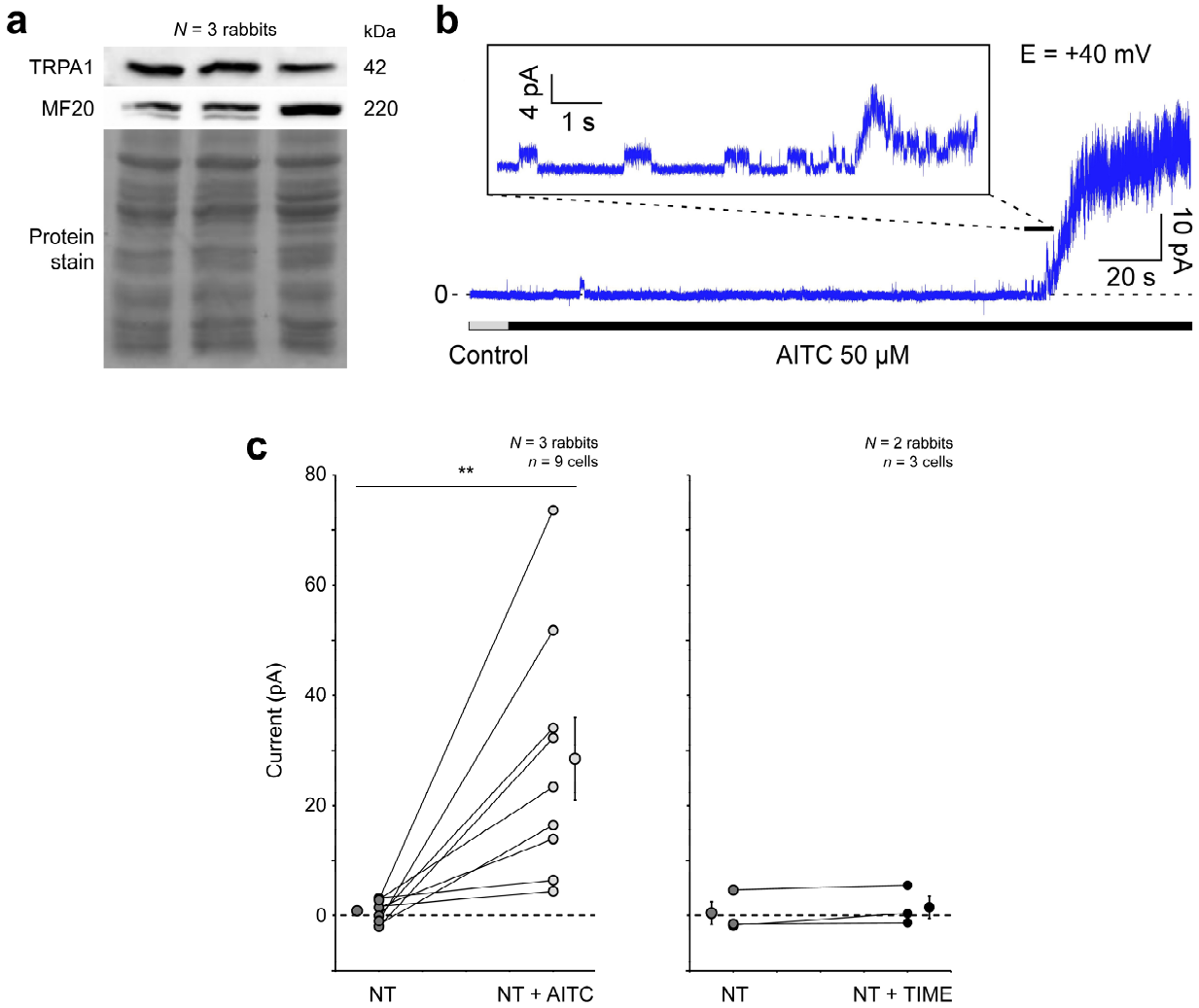

897
898

Extended Data Figure 6 | Effect of pharmacological interventions on mechano-arrhythmogenesis with normal repolarisation-relaxation coupling (RRC). Incidence of arrhythmias (purple) in rabbit isolated left ventricular cardiomyocytes without a pinacidil-induced disruption of RRC, following acute stretch applied during diastole or the vulnerable period (VP_{RRC}) and exposure to one of the following treatments: Tyrode (NT); NT + streptomycin (STP, 50 μM, to non-specifically block mechano-sensitive channels, MSC); NT + HC-030031 (10 μM, to block transient receptor potential ankyrin 1, TRPA1, channels); NT + BAPTA (1 μM, to buffer cytosolic Ca^{2+}, $[Ca^{2+}]_i$), or NT + dantrolene (DNT, 1 μM, to stabilise ryanodine receptors). **Inset,** Of the total arrhythmia incidence (measured as the sum of diastolic and VP_{RRC} incidence), the proportion of arrhythmias that were premature contractions (blue, left) or self-sustained arrhythmic events (shades of red, right), and the effect of blocking either MSC (measured as the pooled stretches in the NT + STP intervention) or chelating $[Ca^{2+}]_i$ (measured as the pooled stretches in the NT + BAPTA intervention) on their incidence. Differences assessed using chi-square contingency tables and Fisher's exact test. *N* = rabbits / group, *n* = cells / group, *m* = stretch stimuli applied.

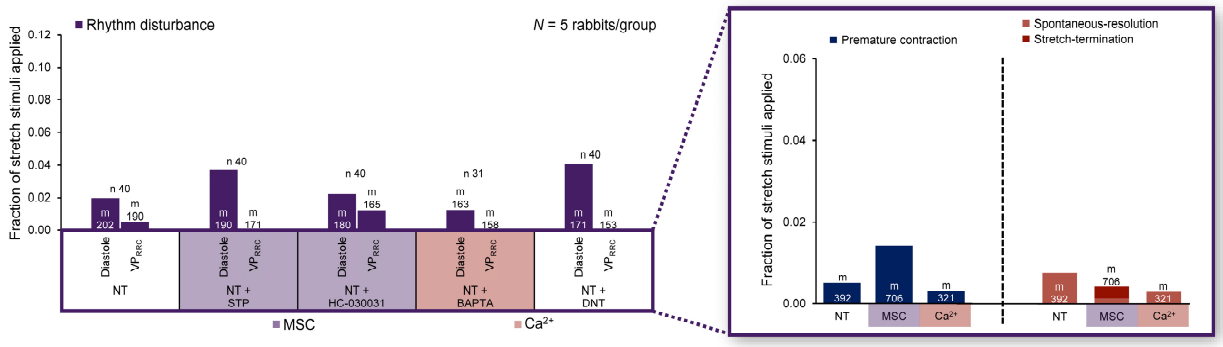

Extended Data Figure 7 | Effect of pharmacological interventions on cellular contractile function in the absence of a pinacidil-induced disturbance of repolarisation-relaxation coupling (RRC). a, Diastolic sarcomere length and **b**, maximum rate and **c**, percent sarcomere shortening during contraction of rabbit isolated left ventricular cardiomyocytes exposed to one of the following conditions: Tyrode (NT); NT + streptomycin (STP, 50 μM, to non-specifically block mechano-sensitive channels); NT + HC-030031 (10 μM, to block TRPA1 channels); NT + BAPTA (1 μM, to buffer cytosolic Ca^{2+}); or NT + dantrolene (DNT, 1 μM, to stabilise ryanodine receptors). Differences assessed by one-way ANOVA, with Tukey *post-hoc* tests for **a** and **b** and by Kruskal-Wallis test for **c**. $*p < 0.05$, $***p < 0.001$. Error bars represent standard error of the mean. N = rabbits / group, n = cells / group.

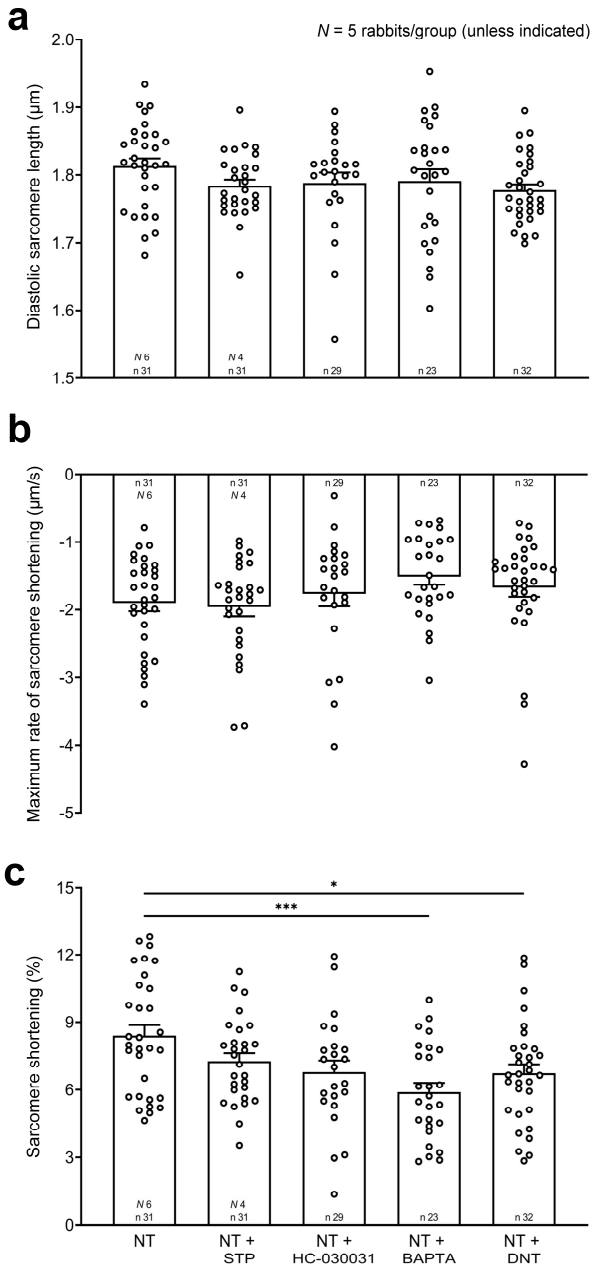

Extended Data Figure 8 | Effect of microtubule density on TRPA1-mediated mechano-arrhythmogenesis. Confocal immunofluorescence images of stained microtubules in rabbit isolated left ventricular cardiomyocytes in either **a,** control conditions (Tyrode, NT) or **b,** following paclitaxel exposure (TAX, 10 μM, to increase the polymerisation and stabilisation of microtubules). **c,** Quantification of microtubule density assessed as the microtubule positive fraction of total cell area. Differences assessed with two-tailed, unpaired Student's t-test. $*p < 0.05$. Error bars represent standard error of the mean. **d,** Incidence of premature contractions (blue) and other self-sustained arrhythmic activity (shades of red) after acute diastolic stretch of rabbit isolated left ventricular cardiomyocytes exposed to one of the following treatments: NT; TAX; or TAX + HC-030031 (10 μM, to block TRPA1 channels). Differences assessed using chi-square contingency tables and Fisher's exact test. $*p < 0.05$, $**p < 0.01$, $***p < 0.001$. N = rabbits / group; n = cells / group, m = stretches.

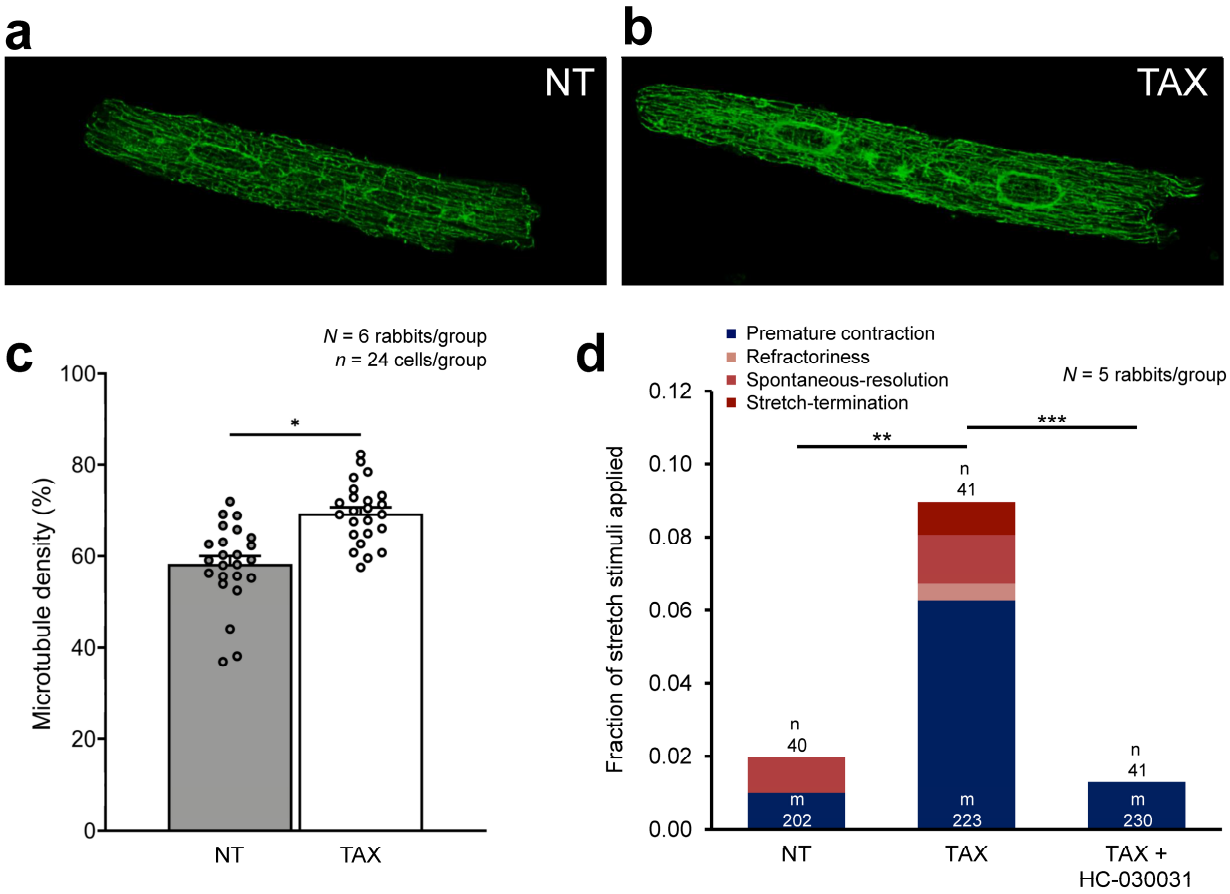

944 **Extended Data Figure 9 | Effect of TRPA1 channel activation on cytosolic Ca^{2+} concentration**
945 **($[Ca^{2+}]_i$).** Percent change in diastolic $[Ca^{2+}]_i$ after exposure to one of the following treatments:
946 pinacidil (PIN, 50 μM, to activate ATP-sensitive potassium channels); allyl isothiocyanate (AITC,
947 50 μM, to activate TRPA1 channels); PIN + HC-030031 (10 μM, to block TRPA1 channels); or
948 AITC + HC-030031. Differences assessed using two-tailed, unpaired Student's t-test between
949 groups within PIN or AITC treatment. *$p < 0.05$. Error bars represent standard error of the mean.
950 N = rabbits / group, n = cells / group.
951

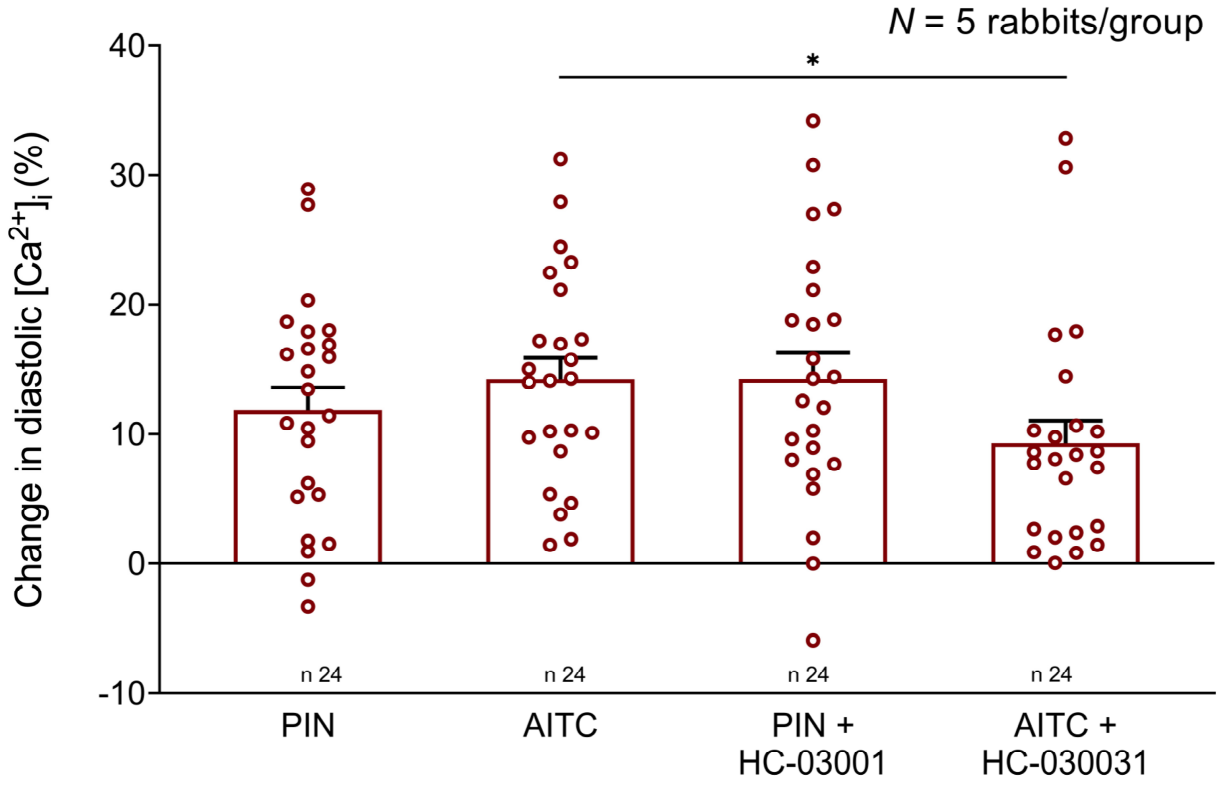

952

Extended Data Figure 10 | Effect of pinacidil (PIN) on cellular mechanics. a, Diastolic (represented by the slope of the end-diastolic stress-length relationship, blue lines with square symbols) and systolic (represented by the slope of the end-systolic stress-length relationship, red lines with round symbols) stiffness of rabbit isolated left ventricular cardiomyocytes either in control conditions (Tyrode, NT; solid lines and filled symbols), or following exposure to PIN (50 µM, to activate ATP-sensitive potassium channels; dashed lines and open symbols). **b,** Calculated diastolic and systolic stiffness, and stiffness-sarcomere length (SL) intercepts in cells exposed to either NT (grey) or PIN (white). Differences assessed using two-tailed, unpaired Student's t-test. $^{**}p < 0.01$, $^{***}p < 0.001$. Error bars represent standard error of the mean. N = rabbits / group, n = cells / group.

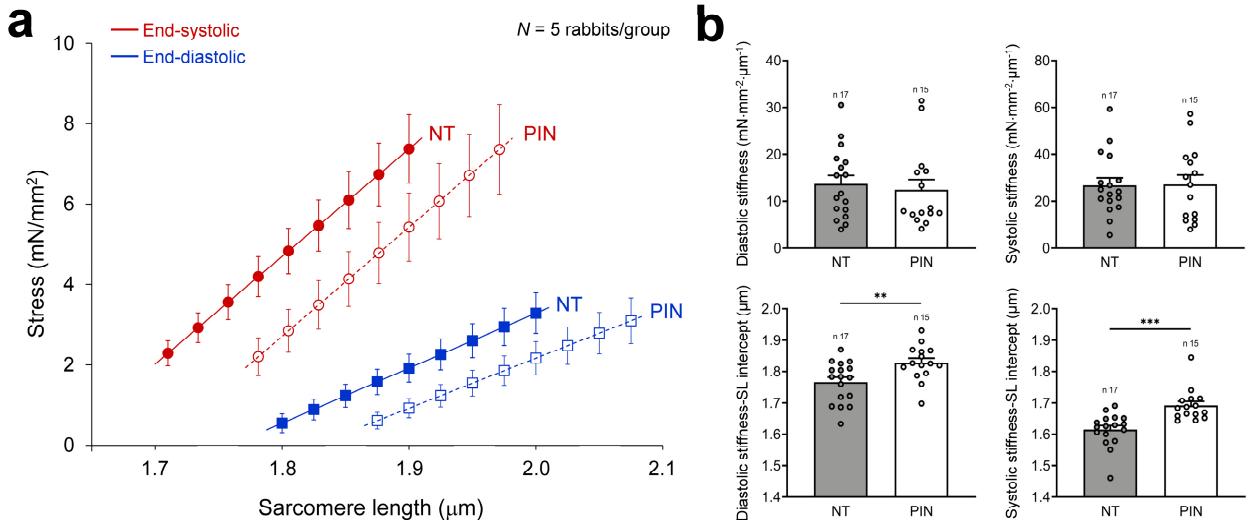

Extended Data Figure 11 | Mechanical characteristics of cell stretch, grouped by timing relative to the electrical cycle and differing electrophysiological outcomes. a, Percent sarcomere stretch, **b,** stretched sarcomere length, and **c,** maximum applied stress in pinacidil-treated (PIN, 50 µM, to activate ATP-sensitive potassium channels) cells for two consecutive acute stretch applications either during diastole or the VP_{RRC}, where one stretch caused an arrhythmia (ARR, red) and the other did not (cell remained in normal paced rhythm, NPR, green), but not always in that order. Differences assessed using the Wilcoxon matched-pairs test. *N* = rabbits / group, *n* = cells / group.

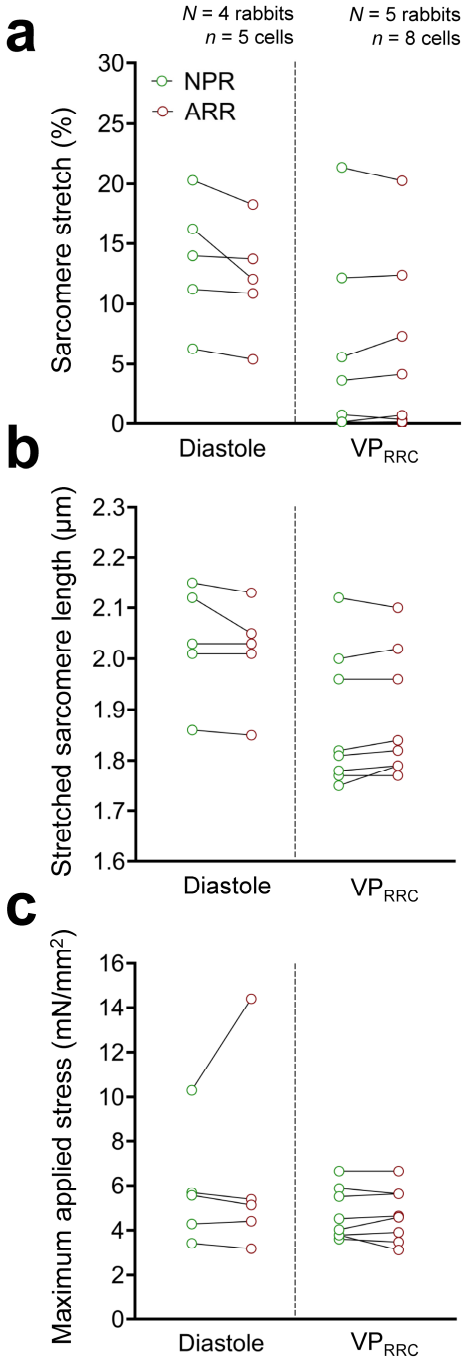

SUPPLEMENTARY INFORMATION

Supplementary Video 1 | Stretch-induced premature contraction. Example of rapid stretch of a rabbit isolated left ventricular myocyte treated with pinacidil (50 μM, to activate ATP-sensitive potassium channels), applied using microscopic carbon fibres adhered to either end of the cell, which resulted in a premature contraction. Sarcomere dynamics and carbon fibre positions were simultaneously measured to assess arrhythmic incidence and confirm maintenance of contractile function (representative sarcomere trace shown in Fig. 2d).

Supplementary Video 2 | Stretch-induced refractoriness. Example of rapid stretch of a rabbit isolated left ventricular myocyte treated with pinacidil (50 μM, to activate ATP-sensitive potassium channels), applied using microscopic carbon fibres adhered to either end of the cell, which resulted in refractoriness. Sarcomere dynamics and carbon fibre positions were simultaneously measured to assess arrhythmic incidence and confirm maintenance of contractile function (representative sarcomere trace shown in Fig. 2f).

Supplementary Video 3 | Stretch-induced sustained arrythmia with termination by stretch. Example of rapid stretch of a rabbit isolated left ventricular myocyte treated with pinacidil (50 μM, to activate ATP-sensitive potassium channels), applied using microscopic carbon fibres adhered to either end of the cell, which resulted in a sustained arrhythmia that was terminated by application of an additional stretch. Sarcomere dynamics and carbon fibre positions were simultaneously measured to assess arrhythmic incidence and confirm maintenance of contractile function (representative sarcomere trace shown in Fig. 2h).

Supplementary Video 4 | Stretch-induced, calcium-driven sustained arrhythmia. Example of simultaneous voltage (blue)-calcium (red) fluorescence imaging in a rabbit isolated ventricular myocyte treated with pinacidil (50 μM, to activate ATP-sensitive potassium channels). Rapid stretch during the vulnerable period (green bar) resulted in sustained arrhythmic activity, in which oscillations in cytosolic calcium preceded changes in voltage, indicating calcium-driven activity (see inset and Fig. 4a).